A novel RIPK2 inhibitor delays NOD signalling complex formation yet prevents inflammatory cytokine production

Ueli Nachbur[1,2], Che A. Stafford[1,2], Aleksandra Bankovacki[1,2], Yifan Zhan[1,2], Lisa M. Lindqvist[1,2], Berthe K. Fiil[3], Yelena Khakham[1,2], Hyun-Ja Ko[1,2], Jarrod J. Sandow[1,2], Hendrik Falk[1,2,4], Jessica K. Holien[5], Diep Chau[1,2], Joanne Hildebrand[1,2], James E. Vince[1,2], Phillip P. Sharp[1,2], Andrew I. Webb[1,2], Katherine A. Jackman[6], Sabrina Mühlen[6], Catherine L. Kennedy[6], Kym N. Lowes[1,2], James M. Murphy[1,2], Mads Gyrd-Hansen[3,8], Michael W. Parker[7,9], Elizabeth L. Hartland[7] , Andrew M. Lew[1,2], David C.S. Huang[1,2], Guillaume Lessene[1,2] and John Silke[1,2*]

[1] The Walter and Eliza Hall Institute of Medical Research, 1G Royal Parade, VIC 3052, Parkville, Australia

[2] Department of Medical Biology, University of Melbourne, Melbourne, Australia

[3] Department of Disease Biology, Novo Nordisk Foundation Center for Protein Research, Faculty of Health and Medical Sciences, University of Copenhagen, DK-2200 Copenhagen, Denmark

[4] Cancer Therapeutics CRC, Bundoora, Victoria, 3083, Australia

[5] ACRF Rational Drug Discovery Centre, St. Vincent's Institute of Medical Research, 9 Princes Street, Fitzroy, Victoria 3065, Australia

[6] The Florey Institute of Neuroscience and Mental Health, Melbourne Brain Centre, Austin Campus, 245 Burgundy Street, Heidelberg, VIC 3084, Australia

[7] Department of Microbiology and Immunology, University of Melbourne, Victoria 3010, Australia

[8] Ludwig Cancer Research, Nuffield Department of Clinical Medicine, University of Oxford, Oxford OX3 7DQ, UK

[9] Department of Biochemistry and Molecular Biology, Bio21 Molecular Science and Biotechnology Institute, University of Melbourne, Parkville, Victoria 3010, Australia

*address for correspondence: Dr John Silke, PhD, The Walter and Eliza Hall Institute of Medical Research, 1G Royal Parade, Parkville, VIC 3052, Australia silke@wehi.edu.au

Intracellular NOD (nucleotide binding and oligomerization domain) receptors recognize antigens including bacterial peptidoglycans and initiate immune responses by triggering the production of pro-inflammatory cytokines through activating NF-κB and MAP (mitogen activated protein) kinases. Receptor Interacting Protein Kinase 2 (RIPK2) is critical for NOD mediated NF-κB activation and cytokine production. We developed and characterized a novel and selective RIPK2 kinase inhibitor, WEHI-345, and show that treatment with this compound delays RIPK2 ubiquitylation and NF-κB activation. Despite only delaying NF-κB activation upon NOD stimulation, WEHI-345 prevents cytokine production *in vitro* and *in vivo*, such that treatment ameliorates experimental autoimmune encephalomyelitis (EAE) in mice. Our study highlights the importance of the kinase activity of RIPK2 for proper immune responses and demonstrates the therapeutic potential of inhibiting RIPK2 in NOD-driven inflammatory diseases.

NOD1 and NOD2 are cytosolic receptors of the innate immune system, able to sense bacterial peptidoglycans from Gram positive and Gram negative bacteria [1-3]. Their function in innate immune responses has been extensively studied, revealing pivotal roles in the host defense against pathogens such as *Listeria monocytogenes, Helicobacter pylori*, and *Staphylococcus aureus* [4-6]. In humans, deregulated NOD signalling due to mutations in NOD receptors, particularly in NOD2, are associated with Crohn's disease, an inflammatory gastro-intestinal disorder [7-9]. Aberrant activation of the NOD pathway can result in Blau syndrome or early onset sarcoidosis, both characterized by familial granulomatous arthritis and skin granulomas [10]. Recently a crucial role for Receptor Interacting Kinase 2 (RIPK2) in promoting infiltration of immune cells into the Central Nervous System (CNS) was reported and RIPK2 deficient mice displayed reduced disease development and progression in a murine model for multiple sclerosis [11].

Once activated, NOD signalling leads to the activation of NF-κB and MAP kinases resulting in the transcription of pro-inflammatory cytokines [12], as well as the induction of autophagy [13]. Multiple components and regulators of the NOD signalling complex have recently been described. RIPK2 plays a central role in the NOD

signalling pathway and cells deficient in RIPK2 fail to mount a cytokine response upon NOD stimulation [14,15]. We and others have shown that upon NOD stimulation, RIPK2 is ubiquitylated by Inhibitor of Apoptosis (IAP) proteins, and this recruits the linear ubiquitination assembly complex (LUBAC), which is essential for downstream signalling [16-18].

While the role of RIPK2 as a NOD adaptor protein and ubiquitylation platform has been established, the biological role and function of RIPK2 as a kinase remains enigmatic. RIPK2 was originally identified as a serine-threonine kinase based on homology [19-21], but has recently been re-classified as a dual-specificity kinase [22]. Earlier reports suggested that the kinase activity of RIPK2 was dispensable for NF-κB activation and cytokine production [23]. On the other hand, a kinase-dead (K47A) knock-in mouse was developed and bone marrow derived macrophages (BMDMs) derived from this mouse were defective in signalling [24], however mutant RIPK2 was not expressed at detectable levels suggesting that kinase activity is required for stable expression rather than signalling per se [24]. Upon activation, RIPK2 auto-phosphorylates on Ser176 and on Tyr474 [22,25]. While Ser176 phosphorylation is essential for RIPK2 activity, phosphorylation of Tyr474 enhances, but is not essential for signalling [22].

Several kinase inhibitors have been described to inhibit RIPK2, albeit non-selectively. Among them are the epidermal growth factor receptor (EGFR) tyrosine kinase inhibitors Gefitinib and Eroltinib [22] and the p38, MAPK and Src inhibitor SB-203580 [26,27]. Pharmacological inhibition of RIPK2 kinase activity via these relatively nonspecific inhibitors, caused a reduction in RIPK2 stability and a reduction in cytokine production upon NOD stimulation. However, these inhibitors also inhibit other kinases in the NOD signalling pathway to varying degrees; therefore, it is difficult to distinguish RIPK2 specific effects. To better understand the role of the kinase activity of RIPK2 in NOD signalling and to explore RIPK2 as a potential therapeutic target we developed a specific and potent RIPK2 inhibitor and tested it *in vitro* and *in vivo*.

RESULTS

WEHI-345 is a potent and selective inhibitor of RIPK2

A potent and specific RIPK2 inhibitor was identified by screening a proprietary library of 120 kinase inhibitors. This compound, WEHI-345 (Fig. 1a), is an ATP analog, and was therefore predicted to bind in the ATP binding pocket of RIPK2.

To gain insights into how WEHI-345 engages the RIPK2 kinase domain, we generated a structural model of the murine RIPK2 kinase domain (residues 18-249), the focus of the present work, using the unpublished X-ray crystal structure of human RIPK2 in complex with ponatinib (PDB: 4C8B) and the Necrostatin-1 bound murine RIPK1 structure (PDB ID: 4ITH [28]) as templates. As is common among inactive protein kinases structures, the hRIPK2 activation loop (residues 165-188) was largely absent, so modelling utilized the structure of murine RIPK1 structure, where only 13 amino acids were absent in this region. The stereochemical quality of the resultant model was assessed via Procheck[29] which showed that over 97% of the amino acids resided in the allowed regions of the Ramachandran plot.

Computational docking of WEHI-345 into this murine RIPK2 homology model is consistent with WEHI-345 occupation of the ATP binding pocket of RIPK2 with hydrogen bonds between the adenosine ring of WEHI-345 and the hinge region residues Glu96 and Met98 of RIPK2 (Fig. 1c). The docking predicts the adenosine ring of WEHI-345 is sandwiched between two leucine residues of RIPK2 (Leu24 and Leu153). There are numerous hydrophobic interactions between the inhibitor and RIPK2 involving residues; Leu24, Ser25, Val32, Ala45, Lys47, Thr95, Tyr97, Met98, Pro99, Asn100, Gly101, Ser102, Glu105 and Leu153, all contributing to the binding affinity between WEHI-345 and RIPK2.

In order to have a less active control in our experiments, we designed a structurally related compound, WEHI-540 (Supplementary Fig. 1a). This compound contained a di-methyl amino group, which was predicted via computational docking to have less hydrophobic interactions with RIPK2 than the pyridine of WEHI-345 (Supplementary Fig. 1b). In a kinase assay, WEHI-345 inhibited the kinase activity of RIPK2 with an

IC_{50} of 130nM (Fig. 1c), while WEHI-540 was approximately 8 fold weaker in inhibiting RIPK2 ($IC_{50=}$ 1.01μM).

The family of RIP kinases is characterized by their relatively conserved kinase domain [30-32]. We therefore tested the activity of WEHI-345 against other RIPKs in a KINOMEscan™. WEHI-345 proved to be highly specific for RIPK2 (K_d=46nM) and displayed negligible activity (>10μM) against RIPK1, RIPK4, and RIPK5 (Fig. 1d). To confirm the absence of activity towards RIPK1, which is also associated with the NODosome [17] and plays an important role in other innate immune signalling pathways, we performed an *in vitro* kinase assay with immunoprecipitated RIPK1 from immortalized mouse BMDMs. Addition of ATP to RIPK1 promoted rapid auto-Ser/Thr phosphorylation and this auto-phosphorylation was blocked by the RIPK1 inhibitor Nec-1. Neither WEHI-345 nor WEHI-540 at a concentration of 1μM were able to prevent auto-phosphorylation of RIPK1 (Supplementary Fig. 1c), indicating a lack of activity towards this kinase.

RIPK3 activity was assessed using Mouse Dermal Fibroblasts (MDFs), treated with a cocktail of TNF, smac-mimetic (cA) and the pan-caspase inhibitor Q-VD-Oph. This treatment induces necroptosis that is dependent on the kinase activities of RIPK1 and RIPK3 and the pseudokinase Mixed Lineage Kinase domain-Like (MLKL) [33-35]. While the RIPK1 inhibitor Necrostatin-1 significantly reduced necroptosis, neither WEHI-345 nor WEHI-540 had any effect on cell death, ruling out activity of WEHI-345 against RIPK1, RIPK3 or MLKL (Supplementary Fig. 1d) at 500nM.

To obtain a complete picture of the inhibitory profile of WEHI-345 in cells we prepared a derivative of WEHI-345, that was linked via an amino group to sepharose beads and used it to precipitate and identify intracellular targets of our drug. Lysates of SILAC labeled THP-1 cells were pre-treated with increasing amounts of unbound WEHI-345 and binding partners in either pre-treated or untreated lysates were precipitated with sepharose bound WEHI-345. Differentially labeled untreated and pre-competed precipitates were then mixed and subjected to analysis by mass spectrometry [36]. Pre-competition with WEHI-345 led to a large increase in the SILAC ratio for RIPK2. Smaller increases were also observed for LYN, HCK, SRC, EPHB1 and MAPK14 (p38) in that order (Figure 1e, supplemental information). Notably, at a

concentration of 1μM of free drug, the only identified target of WEHI-345 was RIPK2. We also tested 92 kinases using KINOMEscan™ (Supplementary Table 1). At a concentration of 1μM, WEHI-345 showed activity of higher than 90% inhibition towards only 4 tested recombinant kinases (KIT, RET, PDGFRß and SRC) and an inhibition of more than 65% for a total of 6 tested kinases (S(35)=0.067). It is worth noting that the 6th strongest hit in the SILAC experiment (MAPK14, p38) was only detected at 100μM of free drug and was not inhibited at all in the KINOMEscan™. Together these data show that WEHI-345 is an highly specific inhibitor for RIPK2 and that in the monocyte cell lines used for NOD assays that RIPK2 is its only real target. Compared to the widely used RIPK2 inhibitors SB-203580 and Erlotinib, WEHI-345 has negligible activity against p38 and EGFR. Inhibition of Src by WEHI-345 is, however, similar to SB-203580 (Supplementary Table 1). Thus WEHI-345 has a superior and unique kinase inhibition profile than previously described inhibitors of RIPK2 in terms of specificity and selectivity.

WEHI-345 is non-cytotoxic and active in cultured cells

Neither WEHI-345 nor WEHI-540 was cytotoxic to BMDMs when used at concentrations up to 1μM, either alone (not shown), or in combination with NOD stimulation (Fig. 2a). To confirm the activity of WEHI-345 in a cellular context, we immunoprecipitated phospho-RIPK2 using a RIPK2 P-Ser176 specific antibody from unstimulated and MDP stimulated cells (Fig. 2b). We were able to immunoprecipitate small amounts of auto-phosphorylated RIPK2 from unstimulated BMDMs; however, addition of MDP markedly increased the amounts of Ser176 phosphorylated RIPK2. Pretreatment with WEHI-345 reduced the levels of P-Ser176-RIPK2 to levels seen in unstimulated cells demonstrating that WEHI-345 is able to inhibit MDP induced autophosphorylation activity of RIPK2 in cells.

We then assessed the role of the kinase activity of RIPK2 in NOD signalling using WEHI-345. THP-1 cells were stably infected with a lentiviral NF-κB GFP reporter and pretreated with WEHI-345 or WEHI-540 before stimulation with either L18-MDP (Fig. 2c) or C12-iE-DAP (Fig. 2d). WEHI-345 reduced reporter activity compared to untreated cells at concentrations above 100nM. As expected, WEHI-345 was more potent than WEHI-540 in inhibiting NOD1 and NOD2 dependent NF-κB activity.

WEHI-345 inhibits cytokine production upon NOD stimulation

WEHI-345 potently blocked MDP induced transcription of the inflammatory mediators TNF and IL-6 in BMDMs (Fig. 3a, b). Similarly, in WEHI-345 treated THP-1 cells stimulated with MDP we observed reduced mRNA levels of NF-κB targets such as TNF, IL-8, IL-1β and A20 (Fig. 3c, d; Supplementary Fig. 2a, b) demonstrating that WEHI-345 inhibits both human and mouse RIPK2 dependent inflammatory cytokine transcription.

MDP-induced secretion of the pro-inflammatory cytokines TNF and IL-6 (Fig. 3e, f) and chemokines MIP-1α, RANTES (Fig. 3g, h) and MCP-1 (Supplementary Fig. 2c) was also potently inhibited at sub-micromolar concentrations of WEHI-345 in IFNγ primed BMDMs. Consistent with our biochemical analysis, WEHI-540 was 10-fold weaker in reducing secretion of cytokines in BMDMs. *Ripk2*$^{-/-}$ BMDMs did not induce any cytokines or chemokines confirming the RIPK2 dependent nature of our NOD stimulation protocol. WEHI-345 also potently inhibited MDP-induced cytokine and chemokine secretion in the mouse macrophage Raw 264.7 cell line (Supplementary Fig. 2d, e).

To test the efficacy of WEHI-345 to inhibit pathogen induced activation of NOD pathways we infected CD11β^{+} monocytes with *Listeria monocytogenes* and measured cytokine secretion in both CCR2^{-} and CCR2^{+} subsets, as this stimulus has been reported to induce RIPK2 dependent cytokine production [5]. In both subsets *Listeria* infection induced a cytokine (represented by TNF) and chemokine (represented by MIP-1α) response when compared to untreated controls (not shown). CCR2^{-} and CCR2^{+} monocytes from RIPK2-deficient animals secreted less cytokines and chemokines upon *Listeria* infection compared to wild-type cells (Supplementary Fig. 2f, g) confirming *Listeria* activates NOD signalling pathways. Consistent with a role for RIPK2 in response to an infection, we observed a trend towards reduced cytokine and chemokine secretion upon WEHI-345 pre-treatment (Fig. 3i, j), that was statistically significant in the case of *Listeria* induced TNF secretion from the CCR2^{+} monocyte population.

As a wide variety of stimuli induce a cytokine response in macrophages and

monocytes, we tested the ability of WEHI-345 to prevent cytokine production by BMDMs induced by other inflammatory stimuli. BMDMs were treated with MDP, TNF, smac-mimetic or LPS; all stimuli that result in cytokine secretion in this cell type, and levels of TNF and IL-6 were measured 24 hours after stimulation (Fig. 4a, b). To enable comparison between stimuli despite their different potency to induce cytokines, we normalized values without inhibitor to 100% secretion for each stimulus. Addition of WEHI-345 significantly reduced the levels of TNF and IL-6 upon MDP stimulation but had no effect on TNF, smac-mimetic or LPS stimulation. We observed a slight decrease of IL-6 levels upon the addition of WEHI-540 after LPS stimulation, however this is unlikely to be due to RIPK2 inhibition. Neither WEHI-345 nor WEHI-540 had any effect on IL-1β production after treatment with the inflammasome stimuli Alum, ATP, smac-mimetic and Staurosporine (Fig. 4c).

In summary, our results demonstrate that WEHI-345 potently and specifically inhibits RIPK2 in cells to prevent NOD induced cytokine production following MDP stimulation or bacterial infection.

RIPK2 inhibition delays NF-κB activation and RIPK2 ubiquitylation

NOD induced NF-κB reporter activity, cytokine mRNA levels and cytokine secretion was almost completely blocked by inhibition of the kinase activity of RIPK2 by WEHI-345. We therefore hypothesized that molecular markers of NF-κB activation would be absent in BMDMs treated with MDP and WEHI-345. To test this we stimulated BMDMs with MDP and generated lysates at several time points post-stimulation (Fig. 5a). Western blots of lysates from MDP stimulated cells revealed a strong and reproducible phosphorylation of p65, IκBα and p38 after 30 minutes. Total IκBα levels were reduced at 60 minutes and returned to normal after 120 minutes, as expected. Intriguingly, given its ability to almost completely block cytokine production, WEHI-345 only delayed rather than blocked MDP induced p65, IκBα and p38 phosphorylation and IκBα degradation. As expected, SB203580, a low nanomolar K_d inhibitor of p38, prevented MDP induced phosphorylation of the p38 target MK-2. SB203580 has also been reported to inhibit RIPK2 and interestingly, had a similar effect to WEHI-345 on the kinetics of IκBα degradation or p65, IκBα and p38 phosphorylation in response to MDP stimulation. To explore these unexpected

observations we performed the same experiment in the THP-1 cell line. As before, we observed a delay rather than a block of molecular markers for NF-κB and MAPK activation following WEHI-345 inhibition, although the inhibitor did reduce phosphorylation of JNK (Fig. 5b). This effect on delayed signalling observed with WEHI-345 was restricted to NOD stimulation and was not observed when cells were stimulated with LPS or TNF, even when a higher concentration of WEHI-345 was used (Fig. 5c).

We and others have previously shown that RIPK2 is potently ubiquitylated upon NOD stimulation, a process that is essential for the recruitment of LUBAC to the signalling complex and efficient downstream signalling [17,37]. We therefore wanted to examine the role of RIPK2 kinase activity for its own ubiquitylation. Blocking RIPK2 kinase activity with WEHI-345 delayed RIPK2 ubiquitylation, which is consistent with the delay in activation of NF-κB in these cells (Fig. 5d). This links the activation of the NF-κB pathway very closely to the ubiquitylation of RIPK2 and suggests a tight crosstalk between kinase activity of RIPK2 and its own ubiquitylation.

IAPs have been shown to be E3 ligases for RIPK2 and to interact with their BIR2 domain with the kinase domain of RIPK2 [37,38]. We therefore tested the hypothesis that WEHI-345 interferes with this interaction. Consistent with these earlier reports, sepharose bound GST did not pull down RIPK2 from THP-1 cells whereas, glutathione sepharose bound GST-BIR2 from either cIAP1 or XIAP pulled down readily detectable amounts of RIPK2 (Figure 5e). However, when cells were pretreated with WEHI-345 before lysis, the amount of RIPK2 that was pulled down by GST-BIR2 of cIAP1 was markedly reduced, indicating that WEHI-345 interferes with cIAP1-RIPK2 interaction (Figure 5e). WEHI-345 was less potent in inhibiting the interaction between RIPK2 and the BIR2 of XIAP.. To test this observation in another manner, we precipitated RIPK2 using GST-BIR2 of cIAP1 and XIAP from untreated THP-1 cells and eluted with either WEHI-345 or the SMAC-mimetic compound A, which binds to the BIR2 domains of IAPs [39]. Compared to compound A, WEHI-345 eluted equal amounts of RIPK2 from GST-BIR2 of cIAP1 and slightly lower amounts from GST-BIR2 of XIAP. These results suggest that WEHI-345 prevents the binding of IAPs to RIPK2, which could explain the delay in RIPK2

ubiquitylation and downstream signalling that we observed.

WEHI-345 desynchronizes NF-κB and AP-1 transcription factors

Cytokine transcription, translation and secretion was almost completely blocked by WEHI-345, however phosphorylation events within the NF-κB and p38 pathways were only delayed. We therefore tested whether the translocation to the nucleus of individual subunits of the NF-κB and activator protein-1 (AP-1) transcription factors was perturbed by WEHI-345 treatment and whether a desynchronization of these transcription factors could explain the loss of cytokine production in WEHI-345 treated cells. THP-1 cells were pre-treated with WEHI-345 for 30 minutes followed by stimulation with L18-MDP for various time points. Cytoplasmic and nuclear extracts were prepared and examined for the NF-κB subunits p65, p50 and RelB as well as the AP-1 subunits cJun, cFos and JunB. All these transcription factor subunits were translocated to the nucleus upon L18-MDP stimulation (Fig. 6a). Consistent with its effects on downstream signalling, WEHI-345 treatment delayed MDP induced nuclear translocation of the NF-κB subunits p65 and p50 and JunB, but there was little evidence for such a delay for the AP-1 subunits cJun and cFos.

This observation suggested that asynchronous activation of essential transcription factors by the NOD signalling pathway could result in a completely defective final response. To test this hypothesis we used a transcription reporter that only requires activation of NF-κB. Asynchronous activation of different transcription factors should not affect transcription from such a reporter vector and as the NF-κB response is only delayed by WEHI-345 we hypothesised that transcription from this reporter vector would also only be delayed. We therefore used THP-1 cells that were stably infected with a lentiviral NF-κB GFP reporter and observed the kinetics of NF-κB activation in the presence or absence of WEHI-345. In accord with the delayed kinetics of p65 phosphorylation and translocation in the nucleus, GFP expression in cells pretreated with WEHI-345 prior to MDP stimulation was only delayed by 30-60 minutes compared to cells that were not treated with WEHI-345 and was not prevented (Fig. 6b). Over time, the levels of GFP increased to a similar extent in both WEHI-345 treated and untreated cells, indicating that even in the presence of WEHI-345, NF-κB is still activated following MDP stimulation.

WEHI-345 blocks MDP induced cytokine production *in vivo*

Pharmacological inhibition of RIPK2 maybe beneficial for the treatment of NOD associated diseases such as multiple sclerosis, Blau syndrome or early onset sarcoidosis where aberrant activation of the NOD pathway can lead to disease [10]. We therefore evaluated WEHI-345 *in vivo*. The pharmacokinetic properties of WEHI-345 were tested following intraperitoneal injection or oral gavage at a dose of 10mg/kg (Fig. 7a). Absorption of both compounds was rapid and maximal plasma concentrations were detected as early as 30 minutes after administration and remained above the analytical limit of quantification (0.5ng mL^{-1}) for 7.5 hours. Intraperitoneal injection resulted in higher maximum plasma concentrations (6.1μM) compared to oral administration (1.2μM). Importantly, no adverse effects after 2 daily injections over 4 days were observed. The maximal tolerated dose was determined to be 25mg kg^{-1} and no pathology or changes on blood cell counts were observed at this dose (not shown).

To test the functionality of WEHI-345 *in vivo* we challenged mice with MDP after pretreatment with WEHI-345. Inflammatory markers such as TNF and MCP-1 were induced in the serum of wild-type mice 4 hours after MDP challenge. Consistent with its function *in vitro*, administration of WEHI-345 reduced levels of TNF and MCP-1 after MDP challenge (Fig. 7b, c). Vehicle treatment did not have an effect compared to PBS injected animals (Supplementary Fig. 3a, b).

WEHI-345 ameliorates EAE in mice

Recently RIPK2 has been implicated in the pathology of chronic progressive experimental autoimmune encephalomyelitis (EAE) because *Ripk2*$^{-/-}$ mice developed a reduced disease score compared to wild-type mice [11]. In two independent experiments, we induced EAE in wild-type C57BL/6 mice and treated with WEHI-345 twice daily (20mg/kg) for 6 consecutive days starting on day 9 after disease induction (Fig. 7d, Supplementary Fig. 3c). In accord with the effect observed in *Ripk2*$^{-/-}$ mice [11], at the conclusion of both experiments (day 23 after disease induction) the mean disease score was significantly lower in WEHI-345 treated animals compared to untreated or vehicle-treated mice. Disease was almost completely prevented (disease score <1) in 5/11 animals by WEHI-345 (Figure 7e). This

establishes RIPK2 kinase as a promising target for the treatment of EAE. Although there was a clear differential between WEHI-345 and vehicle treated mice there was nevertheless a surprising protective effect due to vehicle alone. This prompted us to test another formulation. To reduce unnecessary animal use and obtain additional insight into the role of RIPK2 kinase activity in disease progression we combined this experiment with histological assessment of the CNS, an analysis of cellular composition of the spleen as well as analysis of inflammatory cytokines in mice at the time of onset of disease (day 11, Fig. 7f-j and Supplementary Fig. 4). EAE progression has been reported to be associated with the infiltration of DCs into the CNS around day 17 [11]. We analyzed the forebrain of immunized mice and detected reduced inflammatory infiltrate already at this early time point in the parenchyma in WEHI-345 treated animals (supplementary Figure 4j) and a reduced histological score in WEHI-345 treated animals (Figure 7f). The increase of immune infiltrate to the brain was paralleled by a significant accumulation of splenic pDCs and cDCs in the spleen of WEHI-345 treated animals (Figure 7g,h), while the amounts of $CD4^+$ and $CD8^+$ T cells remained unaltered (Figure 7i,j), suggesting reduced recruitment of dendritic cells to the site of inflammation. We also observed a trend towards improved body weight (Supplementary Fig. 4a) and reduced cytokine and chemokine levels, particularly in the spleen, in WEHI-345 treated mice, indicating overall improvement of the condition (Supplementary Fig. 4b-i).

DISCUSSION

We have identified a novel RIPK2 kinase inhibitor, WEHI-345, that has greater specificity than previously described small molecule kinase inhibitors, such as Erlotinib or SB-203580 that were designed to inhibit other kinases but which show some activity against RIPK2. Unbiased analysis of targets of WEHI-345 in cells and a KINOME scan revealed that WEHI-345 has exquisite specificity for RIPK2. WEHI-345 inhibits RIPK2 activity *in vitro* with an IC_{50} of 134nM while IC_{50} against other RIP Kinases is greater than 10μM. Treatment with WEHI-345 significantly inhibited IL-6 secretion from Raw 267.4 cells at 50nM, showing a 10 fold stronger inhibition than Erlotinib and Gefitinib in an identical assay [22]. In cells, WEHI-345 blocked NOD dependent cytokine production but spared necroptosis signalling mediated by RIPK1 and RIPK3. Smac-mimetic induced activation of IL-1β, that we have recently shown

involves RIPK3 and NLRP3 inflammasome activation [40], was also unaffected by WEHI-345.

Like previously described RIPK2 inhibitors, WEHI-345 targets tyrosine kinases. Although RIP kinases were originally described as Serine/Threonine kinases [41], amino acid sequence alignment suggests RIPK2 is closely related to tyrosine kinases. We here show that WEHI-345 potently inhibits the Serine/Threonine kinase activity of RIPK2.

One of our most striking findings with WEHI-345 was that it only caused a delay in NF-κB transcription factor activation, yet almost completely abrogated cytokine production. The p38 inhibitor SB203580, which also inhibits RIPK2, caused a similar delay in phosphorylation events rather than a complete inhibition after NOD stimulation, supporting the idea that this phenomenon is due to RIPK2 inhibition. Notably, MDP stimulated, NF-κB dependent, production of GFP from a reporter vector matched the NF-κB activation profile and was only delayed reaching similar levels in WEHI-345 and control treated cells after a 45-60 minutes delay. This experiment shows that the NF-κB subunits that translocate into the nucleus in the presence of WEHI-345 are functional and able to induce NF-κB controlled genes. On the other hand, the timing of MDP stimulated nuclear translocation of AP-1 transcription factors was barely affected by WEHI-345 treatment, if at all. This suggests that the delay in NF-κB signalling disrupts the tightly co-ordinated activation of the set of transcription factors that is necessary for complete transcription of inflammatory cytokines.

WEHI-345 inhibited the interaction between RIPK2 and the BIR2 domain of IAPs *In vitro*. All mammalian IAPs: cIAP1, cIAP2 and XIAP have been shown to contribute to NOD signalling[16,17,42] and therefore WEHI-345 could inhibit NOD signalling by binding to the ATP binding pocket of RIPK2 and altering its confirmation so that RIPK2 can no longer bind to IAPs thereby preventing RIPK2 ubiquitylation and downstream signalling events. However in cells, WEHI-345 prevented RIPK2 Ser176 auto-phosphorylation and because phosphorylation of kinases frequently induces a conformational change it is conceivable that phosphorylation drives a conformational

change in RIPK2 that promotes IAP binding and efficient downstream signalling. Our *in vitro* binding experiments were not performed in the presence of MDP and therefore support the first hypothesis. However because we did not compare binding of the phosphorylated and unphosphorylated forms of RIPK2 to the IAPs *in vitro* it is possible that phosphorylation of RIPK2 is a critical regulator of RIPK2/IAP interaction. This is another interesting area for future investigation opened up by our studies.

Whether the observed delay in NF-κB activation is due to incomplete inhibition of RIPK2 kinase activity by WEHI-345 or via an alternative, RIPK2 independent pathway for NF-κB activation remains unclear. Genetic loss of RIPK2 completely abrogates phosphorylation events within the NF-κB pathway after NOD stimulation [43], however unfortunately this does not address this question because ubiquitylation of RIPK2 also provides an essential platform for activation of the IKK1/IKK2/NEMO complex. Competition for the ATP binding site of RIPK2 could result in incomplete inhibition and a delayed activation of downstream signalling. Interestingly, the use of the IAP antagonist compound A also resulted in a delay of phosphorylation events, very similar to the effect observed with WEHI-345[44] and our interaction data suggest that WEHI-345 acts in a similar manner than compound A. This is further evidence that the orchestrated activation of NF-κB and other transcription factors is essential and a perturbation of these transcription factors leads to a total loss of cytokine production. Furthermore it seems to be sufficient to block immediate signalling at the crucial 30 minutes time point for a complete loss of cytokine production.

Finally, we provide evidence that targeting RIPK2 can be beneficial in a murine model for multiple sclerosis. WEHI-345 phenocopied the effect previously observed in RIPK2 deficient mice, even though we treated the mice only upon disease onset and only for 6 days. Despite these limitations we nevertheless prevented disease in almost half of the animals. The lack of efficacy in roughly 50% of WEHI-345 treated animals that developed disease could be due to sub-optimal concentrations of WEHI-345 or that individual mice have a different stage of disease at the beginning of treatment (albeit not clinically evident yet). Surprisingly we observed an effect on disease progression with vehicle alone, confirming the importance of such controls. In

order to delineate the role of RIPK2 it will be necessary to find better formulations that do not have this unanticpated activity and early experiments with a different vehicle formulation suggest that this will be feasible. From a potential treatment perspective it may however be interesting to follow up the role of the vehicle alone. With our second formulation we observed a trend towards reduced cytokine production and overall health of the mice and a significant increase in the amount of dendritic cells in the spleen and decreased inflammatory infiltration in the parenchyma of the forebrain at the onset of disease. This fits with the observations of Shaw et al,[11] who reported a dendritic cell infiltrate to the CNS that was reduced in animals deficient in the NOD signaling pathway. Our results suggest that RIPK2 inhibition results in the retention of DCs in the spleen and therefore in reduced inflammation and ameliorated disease.

In summary WEHI-345 has proven to be an excellent tool compound to specifically investigate the role of the kinase activity of RIPK2 in NOD signalling. It has revealed that asynchronous activation of transcription factors is surprisingly disruptive of cytokine production, uncovered a link between the kinase function of RIPK2 and IAP binding and finally provided evidence that targeting the RIPK2 kinase domain with a small molecule may have therapeutic utility.

MATERIALS AND METHODS

Homology modeling of RIPK2 and in silico docking of ATP and WEHI-345

A homology model of the kinase domain of murine RIPK2 (amino acids 18-249) was constructed using MODELLER 9.11 [45]. The threaded template was constructed using the crystal structures of human RIPK2 structure (PDB ID: 4C8B) and the murine RIPK1 structure with Necrostatin bound (PDB ID: 4ITH, [28]), resulting in a template of over 93% sequence identity. To optimize the model for docking adenosine based compounds, ATP was manually docked into the putative nucleotide binding site, such that it interacted via the adenosine ring to the hinge region of RIPK2 (residues Glu96 and Met98). The resultant structure was then annealed around this site for 10,000 iterations.

The docking of WEHI-345 and WEHI-540 was performed using Surflex within Sybylx2.0 (http://tripos.com/). A protomol was constructed around the putative ATP binding site, with the threshold reduced to 0.28 and the bloat increased to 2Å. Flexibility of the ligand and protein was allowed. The top 20 solutions were retained and visually analysed. Over 80% of the solutions showed a single docking cluster, thus the highest scoring of these was selected as the typical WEHI-345 docking solution. All figures were constructed in Pymol (http://pymol.org/).

RIPK2 biochemical assay

Compounds were tested for inhibition of RIPK2 inhibition using the Transcreener ADP FP assay kit (BellBrook Labs). Briefly, dose-response studies were performed in black Greiner 384-well low volume assay plates in a final volume of 20µL. The substrate peptide (CRRKSLVGTPYWMAPE) and ATP (50µM) were diluted in assay buffer (10mM HEPES pH7.4, 10mM $MgCl_2$, 50µM Na_3VO_4, 0.01% Tween-20, 1mM Dithiothreitol, and 0.01% chicken ovalbumine) and added to the assay plates. Titrations of the test compounds were prepared in DMSO and 0.1µL was added to the substrates by pin tool transfer (PerkinElmer). The recombinant RIPK2 enzyme (Millipore) was diluted in assay buffer and added to start the reactions, with negative controls receiving assay buffer only. After incubation for 90 minutes at 30 degree Celsius the reactions were stopped by adding the detection reagent as per the manufacturer's recommendation. Fluorescence polarisation was read after two hours

on a PerkinElmer EnVision. IC_{50} values were obtained by calculating percent inhibition (%I) for each well relative to controls on the same plate and fitting the data to a four-parameter logistic equation.

Intracellular target identification

THP-1 cells were cultured in lysine and arginine free RPMI supplemented with either normal or heavy (L-Lysine-$^{13}C_6$,$^{15}N_2$ hydrochloride, L-Arginine-$^{13}C_6$,$^{15}N_4$ hydrochloride) lysine and arginine (Sigma) for at least 5 passages prior to the experiment. $21x10^6$ cells of either normal or heavy labeled cells were washed in ice cold PBS and lysed in 1.4mL modified RIPA buffer (1% Nonident P-40, 0.1% Na deoxycholate, 150mM NaCl, 1mM EDTA, 50mM Tris, pH 7.5, 5mM NEM, phosphatase inhibitor cocktail and cOmplete Protease Inhibitor cocktail (Roche)). Lysates were separated and treated with increasing concentrations of WEHI-345 ranging from 0 to 100μM for 20 mins at 4˚C. Following treatment, 20μL of 50:50 S4-conjugated sepharose beads slurry (see supplemental material) were added to each lysate and mixed for 1 hr at 4˚C. Following incubation, beads were spun down (4000g, 1 min, 4˚C) and washed 5 times with cold lysis buffer. Light and heavy samples were then combined and the beads was diluted in 8M and 100 mM Tris-HCl followed by protein digestion with 2μg trypsin according to the previously published FASP protocol [46]. After 16 hours of digestion, peptides were eluted from the filters with 50mM ammonium bicarbonate buffer. Peptides were acidified using 1% formic acid and purified on C18 StageTips (Thermo Scientific) and subjected to LC-MS/MS for relative protein abundancies (see supplemental notes).

KINOMEscan

KINOMEscans were performed by LeadHunter discovery services. Briefly, streptavidin-coated magnetic beads were mixed with biotinylated small molecule ligands to generate affinity resins for the assay. After blocking, binding reactions were assembled by combining DNA tagged kinases, inhibitors and liganded affinity beads. The assay plates were incubated at room temperature for 1hour with constant shaking and the affinity beads were washed. The beads were then resuspended in elution buffer and incubated at room temperature for 30 minutes with shaking. The kinase concentration in the eluates was measured by a quantitative, precise and ultra-sensitive qPCR. The percent inhibition was calculated by measuring the amount of

kinase captured on the solid support as a function of the test compound concentration.

Cell culture and stimulation

HeLa, Raw 264.7 and mouse dermal fibroblasts were maintained in DMEM supplemented with 10% FCS and antibiotics. THP-1 cells were maintained in RPMI medium supplemented with 10% FCS and antibiotics. Bone marrow derived macrophages were generated from wild-type and *Ripk2*$^{-/-}$ mice as previously described [47]. Briefly, the bone marrow from tibiae and femura were cultured for 6 days in DMEM (Invitrogen) supplemented with 10% FCS (GIBCO) and 20% L929 supernatant and antibiotics (Pennicillin, Streptomycin, GIBCO). After 6 days, the cells were detached using Trypsin and replated in 24-,12- or 6-well plates. On the day of stimulation, the cells were either primed with murine IFNγ (5ng/mL, R&D Systems) for 2 hours before the addition of MDP (10μg mL^{-1}, Bachem) or directly stimulated with L18-MDP (100ng mL^{-1}, Invivogen). Fc-hTNF (100nM), Compound A (500nM, TetraLogic Pharmaceuticals) or ultrapure LPS (25ng mL^{-1}, Invivogen) was added to unprimed BMDMs. For inflammasome stimulation, BMDMs were primed with ultra-pure LPS (20ng mL^{-1}) for 3 hours followed by stimulation with Alum (300μg mL^{-1}, 5.5hrs, Thermo Scientific), ATP (5mM, 1.5hrs, Sigma), Compound A (500nM, 5.5hrs) or Staurosporine (1μM, 5.5hrs, Sigma). Necroptosis was induced by treatment with a mix of hFcTNF (100ng mL^{-1}), Compound A (500nM) and Q-VD-Oph (10μM, MP Biochemicals). Necrostatin-1 (50μM, Sigma) was added 30 minutes prior to necroptosis induction. All cells were cultured in 10% CO_2 at 37^{o}C in a humified incubator.

FACS analysis

For cell death assays, MDFs were stained with propidium iodide and fluorescence was assessed on a FACS Calibur (BD). Splenic cell populations were determined by mechanical disruption of one third of the spleen and staining of the cells with anti-CD4 (RM4-5, ebioscience), anti-CD8 (53-6.7, ebioscience) anti-SiglecH (ebio440c, ebioscience) and anti-CD11c (HL3, BD Bioscience). cDCs were defined as CD11c^{high}, SiglecH^{+}, pDCs were defined as CD11c^{intermediate}, SiglecH^{+}.

Monocyte isolation and culture

Heparinized blood of CCR2-CFP reporter mice [48] was suspended in RBC lysis buffer, centrifuged and the cell pellet was washed and resuspended in PBS containing 2% FCS. Washed cells were then stained for cell-surface markers CD11b, Ly6C and Ly6G. CCR2 expression was used for separation of $Ly6C^{+}CCR2^{+}$ and $Ly6C^{-}CCR2^{-}$ monocytes by FACS: For monocyte culture, $2x10^4$ cells were cultured in 0.2mL 10% FCS RPMI (Invitrogen) in a 96-well round bottom plate in the absence or presence of $5x10^6$ *Listeria monocytogenes* for 24 hrs. Culture supernatants were assayed for cytokines and chemokines as described above.

Purification of ubiquitin-conjugates

GST-Tandem Ubiquitin Binding Entities (TUBE1, Lifesensors) were used to purify ubiquitin conjugates from THP-1 cells according to the manufacturers recommendations [49]. THP-1 were lysed in ice cold lysis buffer (100µL per 10^6 cells) and lysates were incubated with TUBEs and affinity resin for 2 hours on ice on a rotating wheel at 4^oC before 3x washing in cold PBS-Tween. Washed beads were resuspended in 1x SDS sample buffer and subjected to Western Blotting.

Western Blotting

After stimulation, cells were directly lysed in 1x SDS sample buffer. DNA was degraded with repeated freeze/boil cycles. For nuclear and cytoplasmic fractionation was performed using NE-PER nuclear protein extraction kit (Pierce) according to the manufacturer's instructions. Total lysates or cytoplasmic and nuclear fractions were run on SDS/PAGE gradient gels, transferred to PVDF or nitrocellulose membrane and blotted with antibodies against total Phospho-p65, ERK, phospho-ERK, phospho-IκBα, total IκBα, phospho-JNK1/2, total JNK1/2, cJun, cFos, GAPDH (all Cell Signalling), Ubiquitin (Imgenex), RIPK2, total p65, JunB, p50, RelB, Lamin A/C (Santa Cruz) and ß-actin (Sigma).

NF-κB activity assay

THP-1 cells were stably transfected with an NF-κB GFP reporter (pTRH NF-κB, System Biosciences). Cells were left untreated or stimulated with either WEHI-345 or

WEHI-450, followed by stimulation with L18-MDP or C12-iE-DAP (Invivogen) for different time points. NF-κB activity was assessed by the mean fluorescence intensity of green cells using Weasel software (WEHI).

Cytokine measurement by ELISA

Cytokines from cell culture supernatants or mouse serum were either measured using Ready-SET-Go! ELISA kits from eBioscience or by Multiplex analysis (BioRad) according to the manufacturers instructions. Mouse sera were diluted up to 1:10 and cell culture supernatants up to 1:2 for TNF and IL-6 and 1:20 for MCP-1 measurements.

qPCR

Total RNA from cultured BMDMs or THP-1 cells at indicated time points was isolated using TRIZOL or the RNeasy Mini Kit (Quiagen) according to the manufacturers instructions. cDNA was synthesized using SuperScript III reverse Transcriptase (Invitrogen) and oigo(d)t primers, in the presence or RNasin (Promega). QPCR was performed using Brilliant III Ultra-Fast SYBR Green QPCR Master Agilent Technologies). Primer sequences were Sense *mmTnf* CATCTTCTCAAAATTCGAGTGACAA; Anti-Sense *mmTnf* TGGGAGTAGA-CAAGGTACAACCC; Sense *mmIl6* CTGCAAGAGACTTCCATCCAGTT; Anti-Sense *mmIl6* GAAGTAGGGAAGGCCGTGG; Sense *hsIL8* GTTCCACTGTGCCTTGGTTT; Anti-Sense *hsIL8* GCTTCCACATGTCCTCACAA; Sense *hsTNF* TGCTGCAGGACTTGAGAAGA; Anti-Sense *hsTNF* GAGGAAGGCCTAAGGTCCAC; Sense *hsA20* ATGCACCGATACACACTGGA; Anti-Sense *hsA20* GGATGATCTCCCGAAACTGA; Sense *hsIL-1β* AAGCTGATGGCCCTAAACAG; Anti-Sense *hsIL-1β* AGGTGCATCGTGCACATAAG; Hypoxanthine phosphoribosyltransferase (*HPRT*; used as reference for normalisation) *hsHPRT* sense AGCCAGACTTTGTTGGATTTG *hsHPRT* anti-sense TTTACTGGCGATGTCAATAGG-3'.

RIPK2-IAP interaction studies

pGEX-6P-3 XIAP BIR2, pGEX-6P-3 cIAP1 BIR2, or pGEX-6P-1 were transformed into BL21 (DE3+) bacteria and grown in Super broth overnight at 37^{o}C. Overnight

culture was diluted 1:10 and grown until OD_{595} was 0.8. IPTG (0.3 mM, Sigma) was added for 4h at 30°C. Cells were pelleted and resuspended in Buffer A (50mM Tris pH 8.0, 50mM NaCl, 1mM EDTA, 1mM DTT, 10% glycerol) and sonicated. After centrifugation at 15 000 rpm for 30 min, the supernatant was incubated with glutathione sepharose 4B (GE Healthcare) for 4h, washed 5 times with Buffer A, and eluted 2X 45 min with 10mM reduced glutathione in Buffer A at 4°C. Elutions were dialysed into Buffer A for storage at -80°C. For pull down experiments, THP-1 cells (10-20 million cells per sample) were washed in PBS and lysed in 0.5 mL MELB (20mM Hepes pH 7.5, 50mM KCl, 2.5mM $MgCl_2$, 1mM EDTA, 250mM sucrose, 0.025% digitonin) with protease inhibitors. After spinning at 13 000 rpm for 5 min, lysates were added directly to 50µL packed glutathione sepharose beads prebound with 60µg GST-BIR2 of human cIAP1, GST-BIR2 of human XIAP, or GST alone. In competition assays, WEHI-345 was added to cells in culture (2µM) for 30 min at 37°C prior to lysis. After incubating on a rotating wheel at 4°C (4h for competition studies, overnight for compound elution studies), beads were washed 3X with 0.5mL MELB without sucrose or digitonin. Beads were either eluted with 2x 0.75µL 25mM glycine pH 2.5 or with 50µM WEHI-345 or compound A.

Pharmacokinetics

Pharmacokinetics of WEHI-345 and WEHI-540 were assessed in non-fasted male Swiss outbred mice after intraperitoneal injection or oral gavage (both 100µL). Triplicate aliquots were taken from the middle of each bulk formulation prior to dosing to confirm concentration. Blood samples were taken at 0.5, 1, 2, 4, and 7.5 hours by submandibular bleed or heart puncture. A maximum of 2 blood samples per mouse were taken. Plasma concentrations in the serum were determined by LC-MS.

In vivo MDP challenge

Mouse colonies were kept under conventional conditions. All experiments with mice were performed according to the guidelines of the animal ethics committee of WEHI, ethics approval # 2011.014. 6-10 week old C57Bl/6 female mice were injected intraperitoneally with WEHI-345 or vehicle control (40% polyethyleneglycol 400 (Sigma), 20% Koliphor HS15 (Sigma), 0.83% benzylalcohol (Sigma)) in a 100µL inoculum. After 30 minutes, mice were challenged with 100µg MDP (Bachem) or with PBS control by another i.p. injection (100µl). The mice were killed by CO_2

asphyxiation 4 hours after MDP treatment and the blood harvested by heart puncture.

Induction and treatment of EAE

EAE was induced as described previously [50]. Briefly, C57BL/6 mice were injected s.c. with 100 μg MOG_{35-55} peptide (Mimotopes) emulsified in complete Freund's adjuvant supplemented with 5 mg/mL heat-killed *Mycobacterium tuberculosis* H37RA (Difco). Mice also received 300 ng pertussis toxin (Sigma) i.v. on days 0 and 2. For disease score studies, mice were either left untreated or i.p. injected twice daily with vehicle or 20 mg/kg WEHI-345, for 6 consecutive days from day 9 after immunization. Neurological impairment was scored daily: 0, no clinical signs; 1, limp tail; 2, hind limb weakness; 3, hind limb paralysis; 3.5, euthanized mouse due to disease score >3 (according to the guidelines of the AEC of WEHI). For the short time study, the vehicle was changed to 12%Capisol® pH 4.0 and treatment was started at day 8 post immunization. 2 daily doses of 20mg kg^{-1} WEHI-345 or vehicle were administered and mice were euthanized 2 hours after the last treatment on day 11 post immunization.

Histological analysis of EAE

11 days post immunization, the brains of untreated, vehicle treated or WEHI-345 treated mice were fixed in 4% paraformaldehyde for at least 48 hours. 3 H&E stained sections of each brain, each 30-50um apart, were analyzed by a double blinded individual and a histological score for each slide was determined based on cellular infiltration to the parenchyma of the forebrain. The histological score per mouse is the average of the three sections of one mouse. Histological scores: 0: minimal to no cellular infiltrate in parenchyma, 1: mild cellular infiltrate in parenchyma, 2: moderate cellular infiltrate to parenchyma, 3: severe cellular infiltrate in parenchyma.

Statistical Analysis

Unless stated otherwise, non-paired Student's t tests were performed for statistical analysis. P values < 0.05 are indicated by *, p values <0.005 by **. P values <0.1 were considered as a trend.

References

1 Chamaillard, M. *et al.* An essential role for NOD1 in host recognition of bacterial peptidoglycan containing diaminopimelic acid. *Nature immunology* **4**, 702-707, doi:10.1038/ni945 (2003).

2 Girardin, S. E. *et al.* Nod1 detects a unique muropeptide from gram-negative bacterial peptidoglycan. *Science* **300**, 1584-1587, doi:10.1126/science.1084677 (2003).

3 Girardin, S. E. *et al.* Nod2 is a general sensor of peptidoglycan through muramyl dipeptide (MDP) detection. *The Journal of biological chemistry* **278**, 8869-8872, doi:10.1074/jbc.C200651200 (2003).

4 Hruz, P. *et al.* NOD2 contributes to cutaneous defense against Staphylococcus aureus through alpha-toxin-dependent innate immune activation. *Proceedings of the National Academy of Sciences of the United States of America* **106**, 12873-12878, doi:10.1073/pnas.0904958106 (2009).

5 Kobayashi, K. *et al.* RICK/Rip2/CARDIAK mediates signalling for receptors of the innate and adaptive immune systems. *Nature* **416**, 194-199, doi:10.1038/416194a (2002).

6 Viala, J. *et al.* Nod1 responds to peptidoglycan delivered by the Helicobacter pylori cag pathogenicity island. *Nature immunology* **5**, 1166-1174, doi:10.1038/ni1131 (2004).

7 Hugot, J. P. *et al.* Association of NOD2 leucine-rich repeat variants with susceptibility to Crohn's disease. *Nature* **411**, 599-603, doi:10.1038/35079107 (2001).

8 Jostins, L. *et al.* Host-microbe interactions have shaped the genetic architecture of inflammatory bowel disease. *Nature* **491**, 119-124, doi:10.1038/nature11582 (2012).

9 Ogura, Y. *et al.* A frameshift mutation in NOD2 associated with susceptibility to Crohn's disease. *Nature* **411**, 603-606, doi:10.1038/35079114 (2001).

10 Henckaerts, L. & Vermeire, S. NOD2/CARD15 disease associations other than Crohn's disease. *Inflammatory bowel diseases* **13**, 235-241, doi:10.1002/ibd.20066 (2007).

11 Shaw, P. J. *et al.* Signaling via the RIP2 adaptor protein in central nervous system-infiltrating dendritic cells promotes inflammation and autoimmunity. *Immunity* **34**, 75-84, doi:10.1016/j.immuni.2010.12.015 (2011).

12 Ogura, Y. *et al.* Nod2, a Nod1/Apaf-1 family member that is restricted to monocytes and activates NF-kappaB. *The Journal of biological chemistry* **276**, 4812-4818, doi:10.1074/jbc.M008072200 (2001).

13 Travassos, L. H. *et al.* Nod1 and Nod2 direct autophagy by recruiting ATG16L1 to the plasma membrane at the site of bacterial entry. *Nature immunology* **11**, 55-62, doi:10.1038/ni.1823 (2010).

14 Hasegawa, M. *et al.* A critical role of RICK/RIP2 polyubiquitination in Nod-induced NF-kappaB activation. *The EMBO journal* **27**, 373-383, doi:10.1038/sj.emboj.7601962 (2008).

15 Magalhaes, J. G. *et al.* Essential role of Rip2 in the modulation of innate and adaptive immunity triggered by Nod1 and Nod2 ligands. *European journal of immunology* **41**, 1445-1455, doi:10.1002/eji.201040827 (2011).

16 Bertrand, M. J. *et al.* Cellular inhibitors of apoptosis cIAP1 and cIAP2 are required for innate immunity signaling by the pattern recognition receptors

NOD1 and NOD2. *Immunity* **30**, 789-801, doi:10.1016/j.immuni.2009.04.011 (2009).

17 Damgaard, R. B. *et al.* The ubiquitin ligase XIAP recruits LUBAC for NOD2 signaling in inflammation and innate immunity. *Molecular cell* **46**, 746-758, doi:10.1016/j.molcel.2012.04.014 (2012).

18 Fiil, B. K. *et al.* OTULIN restricts Met1-linked ubiquitination to control innate immune signaling. *Molecular cell* **50**, 818-830, doi:10.1016/j.molcel.2013.06.004 (2013).

19 Inohara, N., del Peso, L., Koseki, T., Chen, S. & Nunez, G. RICK, a novel protein kinase containing a caspase recruitment domain, interacts with CLARP and regulates CD95-mediated apoptosis. *The Journal of biological chemistry* **273**, 12296-12300 (1998).

20 McCarthy, J. V., Ni, J. & Dixit, V. M. RIP2 is a novel NF-kappaB-activating and cell death-inducing kinase. *The Journal of biological chemistry* **273**, 16968-16975 (1998).

21 Thome, M. *et al.* Identification of CARDIAK, a RIP-like kinase that associates with caspase-1. *Current biology : CB* **8**, 885-888 (1998).

22 Tigno-Aranjuez, J. T., Asara, J. M. & Abbott, D. W. Inhibition of RIP2's tyrosine kinase activity limits NOD2-driven cytokine responses. *Genes & development* **24**, 2666-2677, doi:10.1101/gad.1964410 (2010).

23 Lu, C. *et al.* Participation of Rip2 in lipopolysaccharide signaling is independent of its kinase activity. *The Journal of biological chemistry* **280**, 16278-16283, doi:10.1074/jbc.M410114200 (2005).

24 Nembrini, C. *et al.* The kinase activity of Rip2 determines its stability and consequently Nod1- and Nod2-mediated immune responses. *The Journal of biological chemistry* **284**, 19183-19188, doi:10.1074/jbc.M109.006353 (2009).

25 Dorsch, M. *et al.* Identification of a regulatory autophosphorylation site in the serine-threonine kinase RIP2. *Cellular signalling* **18**, 2223-2229, doi:10.1016/j.cellsig.2006.05.005 (2006).

26 Windheim, M., Lang, C., Peggie, M., Plater, L. A. & Cohen, P. Molecular mechanisms involved in the regulation of cytokine production by muramyl dipeptide. *The Biochemical journal* **404**, 179-190, doi:10.1042/BJ20061704 (2007).

27 Argast, G. M., Fausto, N. & Campbell, J. S. Inhibition of RIP2/RIck/CARDIAK activity by pyridinyl imidazole inhibitors of p38 MAPK. *Molecular and cellular biochemistry* **268**, 129-140 (2005).

28 Xie, T. *et al.* Structural basis of RIP1 inhibition by necrostatins. *Structure* **21**, 493-499, doi:10.1016/j.str.2013.01.016 (2013).

29 Laskowski, R. A., Moss, D. S. & Thornton, J. M. Main-chain bond lengths and bond angles in protein structures. *Journal of molecular biology* **231**, 1049-1067, doi:10.1006/jmbi.1993.1351 (1993).

30 Zhang, D., Lin, J. & Han, J. Receptor-interacting protein (RIP) kinase family. *Cellular & molecular immunology* **7**, 243-249, doi:10.1038/cmi.2010.10 (2010).

31 Meylan, E. & Tschopp, J. The RIP kinases: crucial integrators of cellular stress. *Trends in biochemical sciences* **30**, 151-159, doi:10.1016/j.tibs.2005.01.003 (2005).

32 Festjens, N., Vanden Berghe, T., Cornelis, S. & Vandenabeele, P. RIP1, a kinase on the crossroads of a cell's decision to live or die. *Cell death and differentiation* **14**, 400-410, doi:10.1038/sj.cdd.4402085 (2007).

33 Murphy, J. M. *et al.* The pseudokinase MLKL mediates necroptosis via a molecular switch mechanism. *Immunity* **39**, 443-453, doi:10.1016/j.immuni.2013.06.018 (2013).

34 Sun, L. *et al.* Mixed lineage kinase domain-like protein mediates necrosis signaling downstream of RIP3 kinase. *Cell* **148**, 213-227, doi:10.1016/j.cell.2011.11.031 (2012).

35 Zhao, J. *et al.* Mixed lineage kinase domain-like is a key receptor interacting protein 3 downstream component of TNF-induced necrosis. *Proceedings of the National Academy of Sciences of the United States of America* **109**, 5322-5327, doi:10.1073/pnas.1200012109 (2012).

36 Ong, S. E. *et al.* Identifying the proteins to which small-molecule probes and drugs bind in cells. *Proceedings of the National Academy of Sciences of the United States of America* **106**, 4617-4622, doi:10.1073/pnas.0900191106 (2009).

37 Yang, Y. *et al.* NOD2 pathway activation by MDP or Mycobacterium tuberculosis infection involves the stable polyubiquitination of Rip2. *The Journal of biological chemistry* **282**, 36223-36229, doi:10.1074/jbc.M703079200 (2007).

38 Bertrand, M. J. *et al.* cIAP1/2 are direct E3 ligases conjugating diverse types of ubiquitin chains to receptor interacting proteins kinases 1 to 4 (RIP1-4). *PloS one* **6**, e22356, doi:10.1371/journal.pone.0022356 (2011).

39 Vince, J. E. *et al.* IAP antagonists target cIAP1 to induce TNFalpha-dependent apoptosis. *Cell* **131**, 682-693, doi:10.1016/j.cell.2007.10.037 (2007).

40 Vince, J. E. *et al.* Inhibitor of apoptosis proteins limit RIP3 kinase-dependent interleukin-1 activation. *Immunity* **36**, 215-227, doi:10.1016/j.immuni.2012.01.012 (2012).

41 Hsu, H., Huang, J., Shu, H. B., Baichwal, V. & Goeddel, D. V. TNF-dependent recruitment of the protein kinase RIP to the TNF receptor-1 signaling complex. *Immunity* **4**, 387-396 (1996).

42 Krieg, A. *et al.* XIAP mediates NOD signaling via interaction with RIP2. *Proceedings of the National Academy of Sciences of the United States of America* **106**, 14524-14529, doi:10.1073/pnas.0907131106 (2009).

43 Nachbur, U., Vince, J. E., O'Reilly, L. A., Strasser, A. & Silke, J. Is BID required for NOD signalling? *Nature* **488**, E4-6; discussion E6-8, doi:10.1038/nature11366 (2012).

44 Damgaard, R. B. *et al.* Disease-causing mutations in the XIAP BIR2 domain impair NOD2-dependent immune signalling. *EMBO molecular medicine* **5**, 1278-1295, doi:10.1002/emmm.201303090 (2013).

45 Sali, A. & Blundell, T. L. Comparative protein modelling by satisfaction of spatial restraints. *Journal of molecular biology* **234**, 779-815, doi:10.1006/jmbi.1993.1626 (1993).

46 Wisniewski, J. R., Zougman, A. & Mann, M. Combination of FASP and StageTip-based fractionation allows in-depth analysis of the hippocampal membrane proteome. *Journal of proteome research* **8**, 5674-5678, doi:10.1021/pr900748n (2009).

47 Hammer, M. *et al.* Control of dual-specificity phosphatase-1 expression in activated macrophages by IL-10. *European journal of immunology* **35**, 2991-3001, doi:10.1002/eji.200526192 (2005).
48 Hohl, T. M. *et al.* Inflammatory monocytes facilitate adaptive CD4 T cell responses during respiratory fungal infection. *Cell host & microbe* **6**, 470-481, doi:10.1016/j.chom.2009.10.007 (2009).
49 Hjerpe, R. *et al.* Efficient protection and isolation of ubiquitylated proteins using tandem ubiquitin-binding entities. *EMBO reports* **10**, 1250-1258, doi:10.1038/embor.2009.192 (2009).
50 Ko, H. J. *et al.* Transplantation of autoimmune regulator-encoding bone marrow cells delays the onset of experimental autoimmune encephalomyelitis. *European journal of immunology* **40**, 3499-3509, doi:10.1002/eji.201040679 (2010).

Acknowledgements

We thank Prof. R. Flavell for the gift of *Ripk2*$^{-/-}$ mice, Prof. C. Day for the gift of GST-BIR2 constructs, M. Rashidi for THP-1 NF-κB GFP reporter cells and K. Trueman, K. Vella and R. Poppelton for assistance with animal work. The work was supported by the NHMRC (grants 1046986, 461221, 1016701, 1037321, 1043414, 1024839, 1035502, 1051210, 606788, a CJ Martin fellowship to KAJ and research fellowships to JS, JV, LML, MWP and DCSH), the ARC (fellowships to UN (FT130100166), JMM (FT 100100100), the WEHI de Burgh Fellowship to GL, the Rebecca Cooper Foundation, the Juvenile Diabetes Research Foundation; the Leukaemia and Lymphoma Society, the Australian Cancer Research Foundation, Catalyst Therapeutics, the Novo Nordisk Foundation and the Lundbeck Foundation. UN was also supported by the Swiss National Science Foundation (SNSF, fellowship #PA00P3_126249). MGH was supported by a Steno Fellowship from the Danish Council for Independent Research – Natural Sciences. JKH is supported by a joint Cure Cancer/ Leukemia Foundation Fellowship. LML is a Bisby Fellow and thanks the CIHR for a Post-PhD Fellowship. This work was made possible through Victorian State Government Operational Infrastructure Support and Australian Government NHMRC IRIISS (#361646).

Author contributions

U.N., C.A.S., A.B., Y.Z., L.M.L., B.K.F., Y.K., H.J.K., J.J.S., H.F., J.K.H., D.C., J.H., J.E.V., P.P.S, A.I.W, S.M., C.L.K., K.N.L. and J.M.M. designed and performed experiments. U.N., J.M.M., M.G.H., M.W.P., E.L.H., A.M.L., D.C.S.H., G.L. and J.S. analyzed data, provided helpful suggestions and discussions. U.N., G.L. and J.S. designed the study and wrote the manuscript.

FIGURE LEGENDS

Figure 1: WEHI-345 is a selective inhibitor of RIPK2. (a) Chemical structure of WEHI-345. **(b)** Model of WEHI-345 docked into the putative ATP binding pocket of RIPK2. Displayed are the amino acids (shown as a line representation), which interact with WEHI-345 (shown as stick representation). Color coding: carbon in grey for RIP2 and cyan for WEHI-345, hydrogen in gray, oxygen in red, nitrogen in blue and sulfur in yellow. hydrogen bonds are highlighted as yellow dashed lines. **(c)** *In vitro* kinase assay using recombinant RIPK2. Values were normalized to RIPK2 activity in the absence of inhibitor. IC_{50}(WEHI-345)=0.13μM, IC_{50}(WEHI-540)=1.01μM. Technical duplicates of one out of 3 assays are shown. **(d)** Inhibition of RIP kinases by WEHI-345 determined by i*n vitro* kinase assay using recombinant RIPK1, -2, -4 and -5. **(e)** SILAC labeled THP-1 cells were lysed and treated with increasing concentrations of WEHI-345 before precipitation with Sepharose bound WEHI-345. SILAC ratios of the 6 strongest binders are shown as average and range of 2 technical repeats. For complete results, see supplementary information.

Figure 2: WEHI-345 does not induce cell death and inhibits RIPK2 activity in cells. **(a)** Cell survival of WEHI-345 and WEHI-540 was assessed on MDP stimulated BMDMs using PI staining and flow cytometry 24 hours after treatment. n=3. **(b)** Raw 267.4 cells were either left untreated, treated with 10μg mL^{-1} MDP or with 500nM WEHI345 and MDP. Lysates were immunoprecipitated using a P-Ser176 specific RIPK2 antibody. Levels of RIPK2 in lysates and immunoprecipitations were determined using Western Blot for total RIPK2. One representative experiment of 3 repeats is shown. **(c,d)** *In vitro* activity of WEHI-345 and WEHI-540 in L18-MDP (200ng mL^{-1}) (d) or C-12 DAP (1μg mL^{-1}) (e) stimulated THP-1 cells was tested using a NF-κB-GFP reporter assay. Values were normalized to untreated (0%) and L18-MDP respectively C12-iE-DAP treated cells (100%). n≥3. Error bars are SEM.

Figure 3: WEHI-345 blocks cytokine transcription and secretion upon NOD stimulation and bacterial infection. (a,b) IFNγ primed BMDMs from wild-type or *Ripk2*$^{-/-}$ mice were stimulated with 10μg per mL MDP in the absence or presence of WEHI-345 (500nM) and RNA levels of TNF (a) and IL-6 (b) were determined using RTQPCR. n = 3. **(c,d)** THP-1 cells were stimulated with 200ng mL^{-1} L18-MDP in the presence or absence of WEHI-345 (2μM) and mRNA levels of TNF (c) and IL-8 (d)

were determined using RTPCR, n = 3, target accumulation at 2h in L18-MDP + vehicle-treated cells was set to 100%. **(e,f)** IFNγ primed wild-type BMDMs (n = 6) were treated with increasing concentrations of WEHI-345 for 30 minutes before the addition of MDP and levels of TNF (e), and IL-6 (f), were measured using ELISA 24 hours after the addition of MDP. $RIPK2^{-/-}$ BMDMs (n = 1) were used as a negative control. **(g,h)** MIP-1α (g) and RANTES (h) levels in the supernatant of IFNγ primed BMDMs were measured from untreated, MDP (10μg mL^{-1}) stimulated or WEHI-345 (500nM) + MDP treated BMDMs of wild-type mice (n = 3). **(i,j)** $CCR2^{+}$ and $CCR2^{-}$ monocytes were infected with *Listeria monocytogenes* and cytokine levels in the supernatant were measured using Bioplex analysis. Error bars are SEM.

Figure 4: WEHI-345 specifically blocks cytokine production upon NOD stimulation. (a,b) wild-type BMDMs were treated with IFNγ+MDP (10μg mL^{-1}), TNF (100ng mL^{-1}), Smac mimetic (compound A, 500nM) or LPS (2.5ng mL^{-1}). Cytokine levels of TNF (a, n=6-9) and IL-6 (b, n=3-6) were determined after 24 hours by ELISA. Values were normalized to the average of control samples for better comparison. Absolute values of control samples for TNF (a) were: MDP: 142pg/mL, TNF: 29pg mL^{-1}, cA: 446pg mL^{-1}, LPS: 3.9 ng mL^{-1}) and for IL-6 (b): MDP: 29pg mL^{-1}, TNF: 61pg mL^{-1}, cA: 188pg mL^{-1}, LPS: 12.9 ng mL^{-1}).

(c) The inflammasome in LPS primed wild-type BMDMs were activated using Alum (250μg mL^{-1}), ATP (5mM), Smac mimetic (Compound A, 500nM) or Staurosporine (1μM), and levels of IL-1β in the supernatant was measured by ELISA. Values were normalized to the average of control samples (Alum: 508pg mL^{-1}, ATP: 220pg mL^{-1}, compound A: 230pg mL^{-1}, Staurosporine: 124pg mL^{-1}). n=3-4. Error bars are SEM.

Figure 5: Inhibition of RIPK2 activity substantially delays NF-κB signalling and RIPK2 ubiquitination upon NOD stimulation by interfering with IAP-RIPK2 interaction. **(a)** IFNγ primed wild-type BMDMs were either left untreated, treated with 500nM WEHI-345 or SB-203580 30 minutes before the addition of 10μg/mL MDP. Cell lysates were taken at indicated time points after the addition of MDP and probed with the indicated antibodies. Probing for RIPK2 confirmed the genotype and β-actin blot was used as a loading control. One experiment out of 6 biologically independent cultures of BMDMs is shown. **(b)** THP-1 cells were either treated with

WEHI-345 (2mM) or left untreated 30 minutes before the addition of L18-MDP (200nM). Cell lysates were taken at the indicated time points and probed for Phospho-IκBα, total-IκBα, Phospho-JNK1/2 and total JNK1/2 as a measure for NF-κB and MAPK activation. Actin was used as a loading control. One experiment out of 3 independent repeats is shown. **(c)** Wild-type BMDMs were either left untreated, treated with 1μM WEHI-345 or WEHI-540 30 minutes before stimulation with IFNγ+MDP, LPS or TNF. Cell lysates from indicated time points were probed for NF-κB and MAPK activation with the indicated antibodies. One experiment out of 6 biologically independent cultures of BMDMs is shown. **(d)** THP-1 cells, either left untreated or pretreated with WEHI-345, were stimulated with L18-MDP for the indicated time points and ubiquitin conjugates were purified using TUBEs. Lysates and pull downs were tested by Western blot using the indicated antibodies. One experiment out of 2 independent repeats is shown. **(e)** THP-1 cells were either left untreated or treated with WEHI-345 for 30 minutes before lysis. RIPK2 was precipitated using sepharose bound GST-BIR2 of cIAP1 or XIAP or GST alone and levels of precipitated RIPK2 was determined by Western Blot. Ponceau staining serves as a loading control for protein loading and GST conjugates. **(f)** RIPK2 was precipitated from THP-1 cells with sepharose bound GST-BIR2 of cIAP1 or XIAP and eluted using DMSO, WEHI-345 or the SMAC mimetic, compound A (upper panel), followed by SDS elution (lower panel).

Figure 6: WEHI-345 desynchronizes NF-κB and AP-1 transcription factors. (a) THP-1 cells were stimulated with 200ng mL^{-1} L18-MDP for the indicated time points, cytoplasmic and nuclear fractions were prepared and probed by Western Blot with the indicated antibodies. **(b)** THP-1 NF-κB GFP reporter cells were either left untreated or treated with WEHI-345 (500nM) 30 minutes before the addition of L18-MDP (200ng mL^{-1}). MFI (GFP) was measured at the indicated time points. Error bars are SEM.

Figure 7 WEHI-345 inhibits NOD signalling in vivo and has a beneficial effect on an EAE model. (a) Bioavailability of WEHI-345 after i.p. or oral administration in non-fasted male Swiss outbred mice (n = 2 for each time point). **(b,c)** C57BL/6 mice were pretreated for 30 minutes with either vehicle or WEHI-345 (100μl, i.p. injection), followed be challenge with MDP (5mg kg^{-1}, i.p. injection) for 4 hours.

Serum levels of TNF (b) and MCP-1 (c) were determined using ELISA. n = 12 for all wild-type groups, n = 7 for *Ripk2*$^{-/-}$. Error bars are SEM **(d)** EAE was induced in wild-type C57 Bl/6 mice and from day 9 after disease induction, mice were treated twice daily with 20 mg kg^{-1} WEHI-345 for 6 days. The clinical score of each mouse was assessed daily and mice were followed up to day 23. The mean clinical score ± SEM of one experiment is shown. Control: n = 6, vehicle: n = 5, WEHI-345: n = 6. **(e)** Clinical scores of two independent EAE experiments at d23 post disease induction. Individual scores as well as the mean score of two independent experiments are shown. Control: n = 10, vehicle: n = 13, WEHI-345: n = 11. Control vs vehicle: p=0.620, control vs WEHI-345: p=0.017, vehicle vs WEHI-345: p=0.029. **(f)** Histological score of forebrain sections of untreated, vehicle or WEHI-345 treated mice 11 days after EAE induction using an improved formulation for WEHI-345. Control: n = 6, vehicle: n = 6, WEHI-345: n = 6. Control vs vehicle: p=0.290, control vs WEHI-345: p=0.064, vehicle vs WEHI-345: p=0.034. **(g-j)** splenic cellularity of untreated, vehicle or WEHI-345 treated mice at day 11 post immunization. Control: n = 6, vehicle: n = 6, WEHI-345: n = 6. Shown are individual values, averages and error bars are SEM.

Supplementary Figure 1: WEHI-345 and WEHI-540 are inhibitors of RIPK2**. (a)** Chemical structure of WEHI-540 **(b)** Models of WEHI-345 (cyan carbons) and WEHI-540 (peach carbons) docked into the putative ATP binding pocket of RIPK2 (white carbons). Displayed are the amino acids which interact with WEHI-345 and hydrogen bonds are highlighted as yellow dashed lines. WEHI-540 is not able to interact with amino acids Tyr97, Pro99 and Asn100 thus was predicted to be a less active RIPK2 inhibitor. **(c)** In vitro kinase assay using endogenous RIPK1 from immortalized mouse BMDMs. Nec-1 potently inhibited P-Thr autophosphorylation of RIPK1 while WEHI345 and WEHI540 did not alter autophosphorylation of RIPK1. Shown is one experiment of at least 3 independent repeats **(d)** SV40 immortalized mouse dermal fibroblasts were either left untreated or treated with TNF, SMAC mimetic (Compound A, cA) and QVD to induce necroptosis. Addition of Nec-1 reduced the amount of cell death but WEHI345 or WEHI540 did not alter cell death. n = 6. Error bars are SEM.

Supplementary Figure 2: WEHI-345 blocks cytokine transcription and secretion upon NOD stimulation and bacterial infection **(a,b)** THP-1 cells were stimulated with L18-MDP in the presence or absence of WEHI-345 (2 μM) and mRNA levels of IL-1β (a) and A20 (b) were determined using RTPCR, n = 3 . **(c)** IFNγ primed wild-type BMDMs (n = 6) were treated with increasing concentrations of WEHI-345 before the addition of MDP and levels of MCP-1 were measured using ELISA 24 hours after the addition of MDP. *ripk2*$^{-/-}$ BMDMs (n=1) were used as a negative control. (**d,e**) Raw 267.4 cells were either left untreated or pretreated WEHI-345 or WEHI-540 before the addition of and MDP. Levels of TNF (d) and IL-6 (e) were measured by ELISA. n=3. Error bars are SEM. **(f,g)** CCR2^{+} and CCR2^{-} monocytes of either wild-type or *ripk2*$^{-/-}$ mice were infected with *Listeria monocytogenes* and levels of TNF (f) or MIP-1a (g) in the supernatant were measured using Bioplex analysis. n=4. Error bars are SEM.

Supplementary Figure 3: WEHI-345 blocks cytokine secretion in vivo and ameliorates EAE **(a,b)** C57Bl/6 mice were challenged for 4 hours with MDP after pretreatment with either PBS, vehicle or 25 mg kg^{-1} WEHI-345 and serum levels of TNF (a) and MCP-1 (b) were determined using ELISA. n = 4 (PBS) or n = 5 (vehicle,

WEHI-345). Error bars are SEM. **(c)** EAE was induced in wild-type C57 Bl/6 mice. On day 9 after disease induction, mice were treated twice daily with 20 mg kg^{-1} WEHI-345. The clinical score of each mouse was assessed daily and mice were followed up to day 23 after disease induction. control: n = 4, vehicle: n = 8, WEHI-345 :n = 5. The mean clinical score ± SEM of one experiment is shown.

Supplementary Figure 4 WEHI-345 reduces weight loss and cytokine secretion in EAE using a new formulation. **(a)** EAE was induced in wild-type C57 Bl/6 mice and mouse weights at day 11 post immunization indicate a trend towards improved health condition in WEHI-345 treated mice. control: n = 6, vehicle: n = 6, WEHI-345: n = 6. Shown are individual values, averages and error bars are SEM. untreated vs vehicle: p=0.489, untreated vs WEHI-345: p=0.074, vehicle vs WEHI-345: p=0.085 (**b-i**) Cytokine and chemokine levels in the spleen and in the serum were measured at day 11 after immunization in the animals as in (a). There is a trend towards reduced cytokine and chemokine production in WEHI-345 treated mice (white bars). control: n = 6, vehicle: n = 6, WEHI-345: n = 6. Shown is the average and error bars are SEM as well as p values for vehicle vs WEHI-345 in the spleen. (j) Representative sections of the forebrain of untreated (control), vehicle treated or WEHI-345 treated mice at day 11 after immunization. Parenchymal cellular infiltrate is reduced in WEHI-345 treated mice compared to control or untreated animals. Scale bar = 500 μm.

Supplementary Table 1: Inhibition of kinases by WEHI-345. A KINOMEscan for 96 kinases was performed using WEHI-345 at a concentration of 1 μM. Listed is the % inhibition for each kinase. Kinases inhibited more than 95% are highlighted in bold.

Supplementary Table 2: Disease scores of the first repeat of the EAE experiment

Supplementary Table 3: Disease scores of the second repeat of the EAE experiment

Nachbur et al, Figure 1

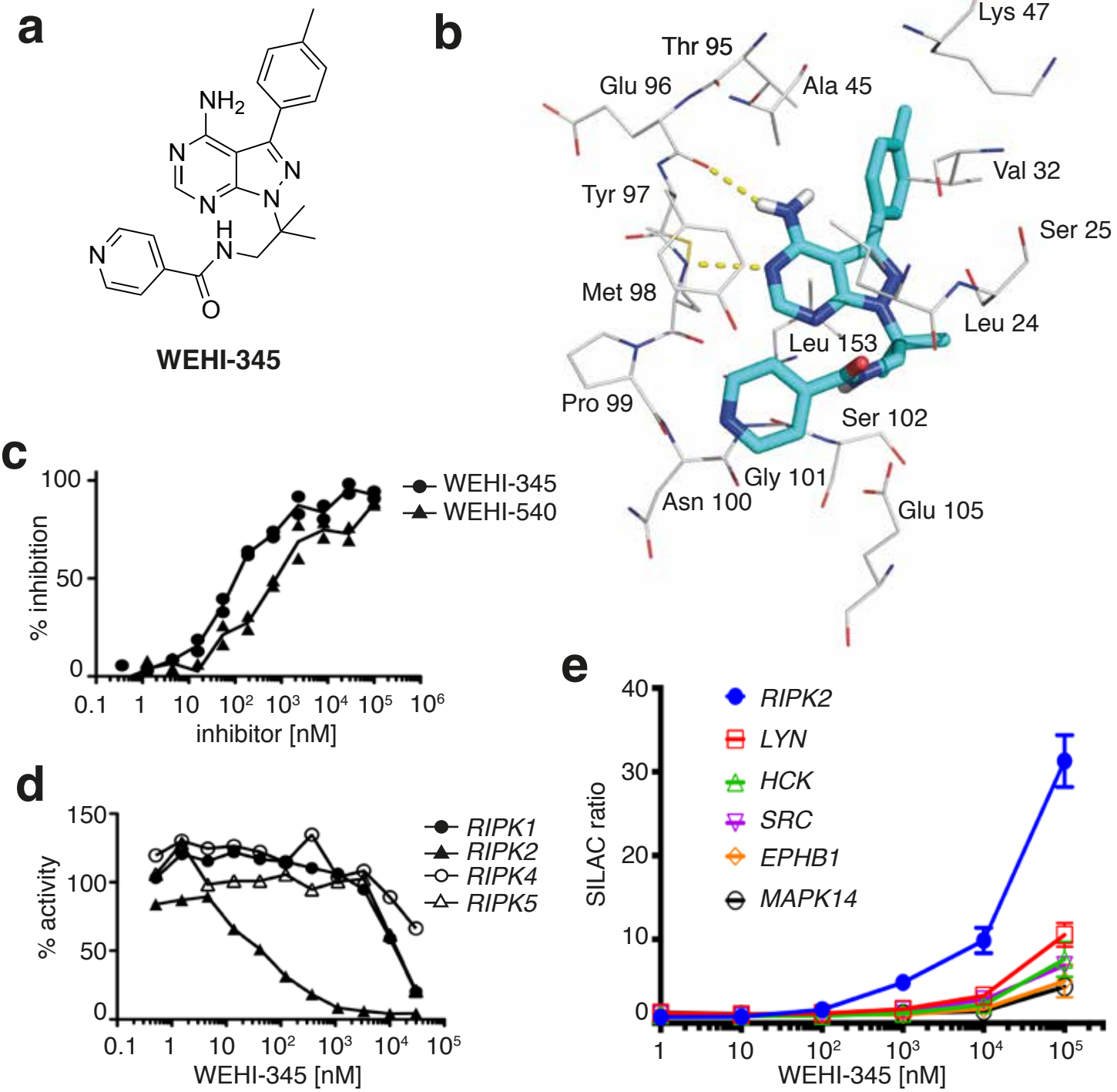

Nachbur et al, Figure 2

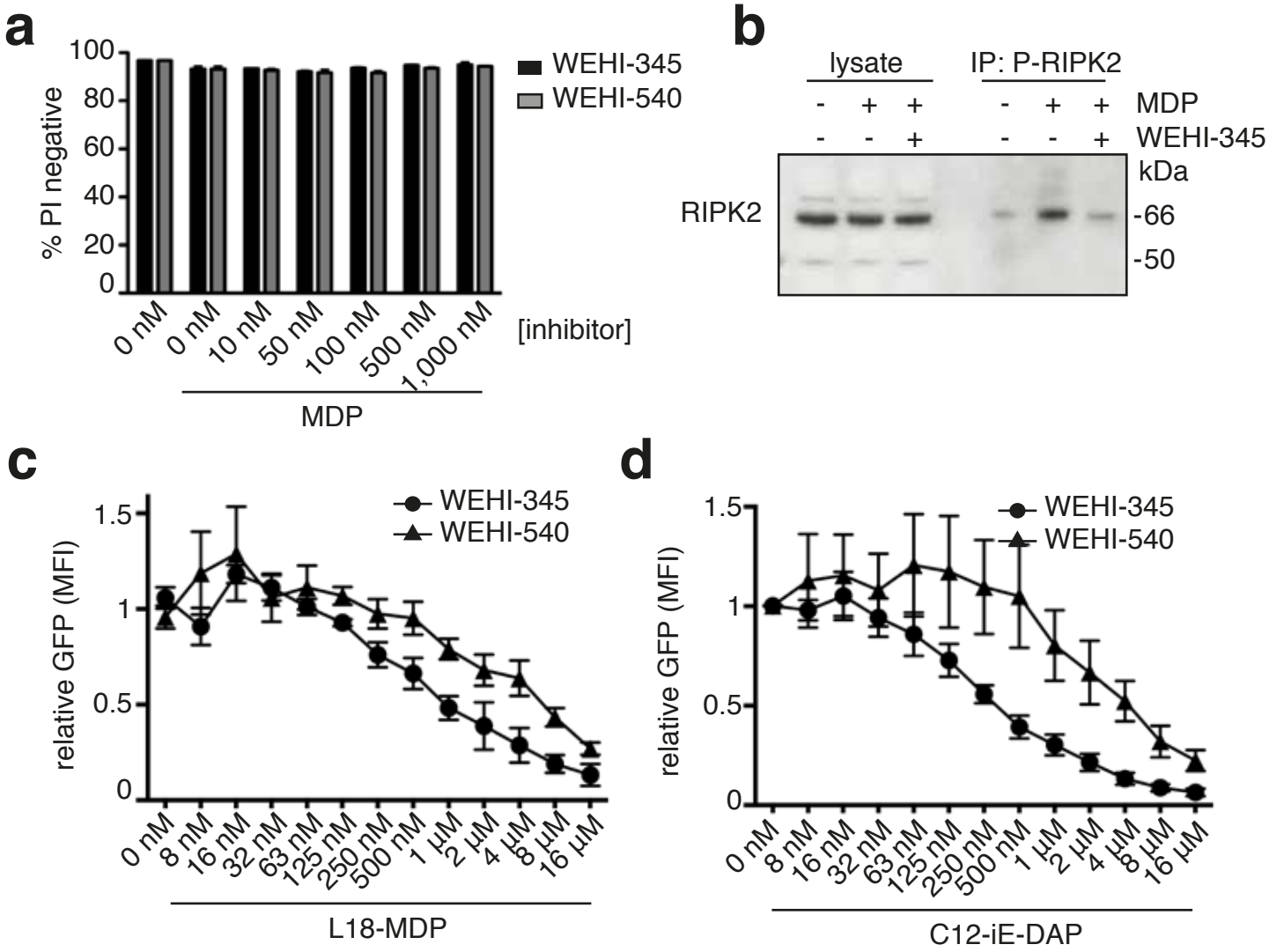

Nachbur et al, Figure 3

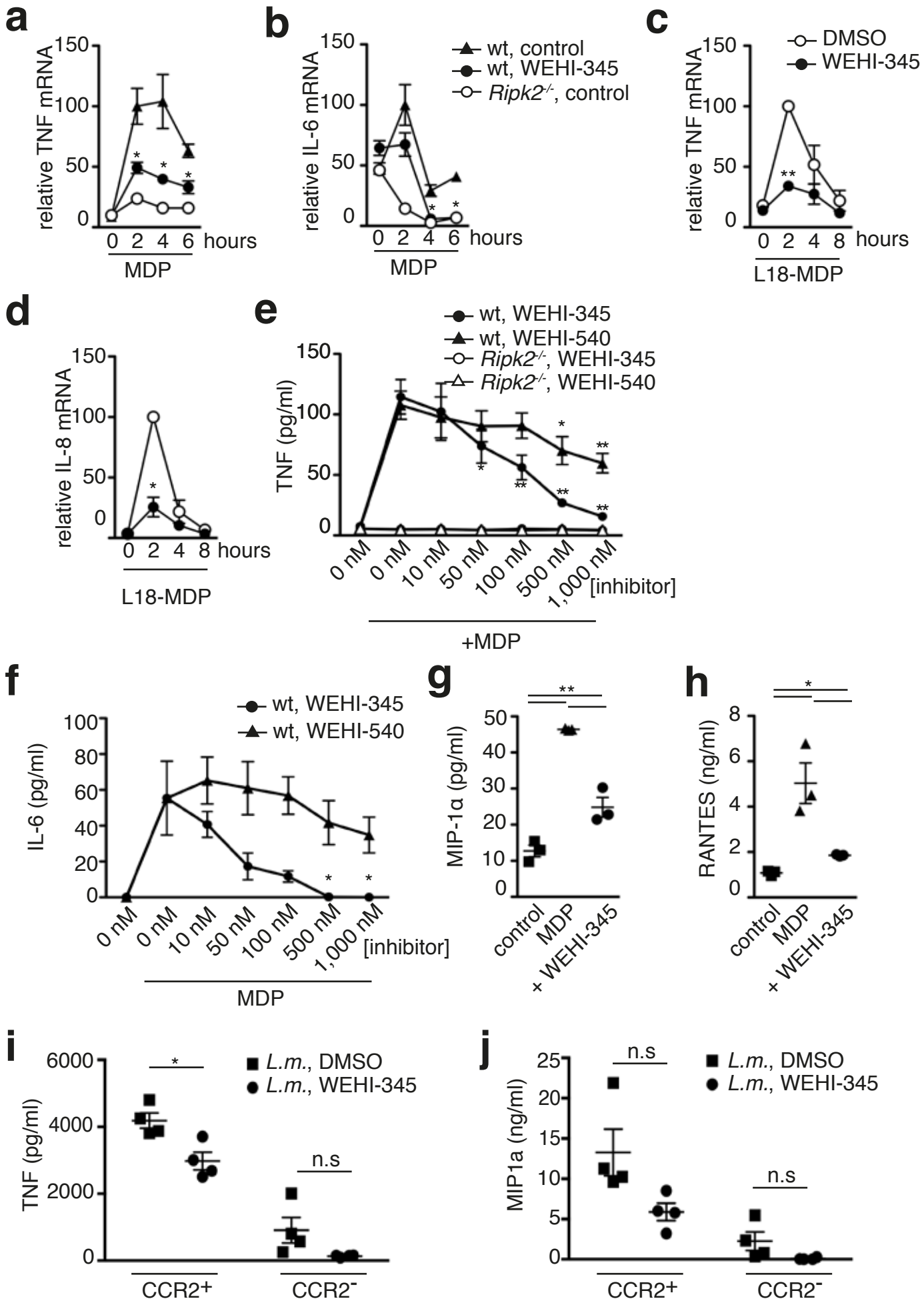

Nachbur et al, Figure 4

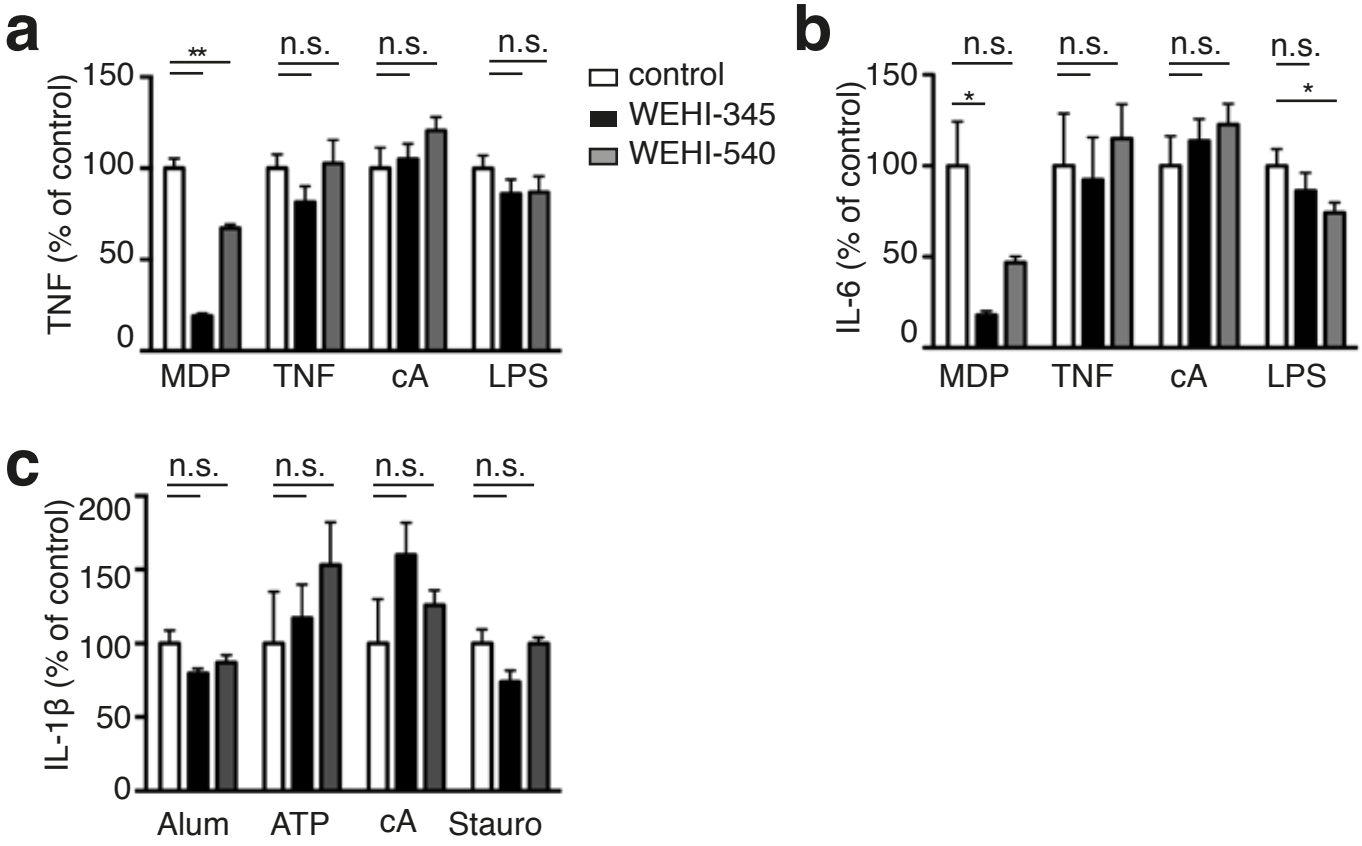

Nachbur et al, Figure 5

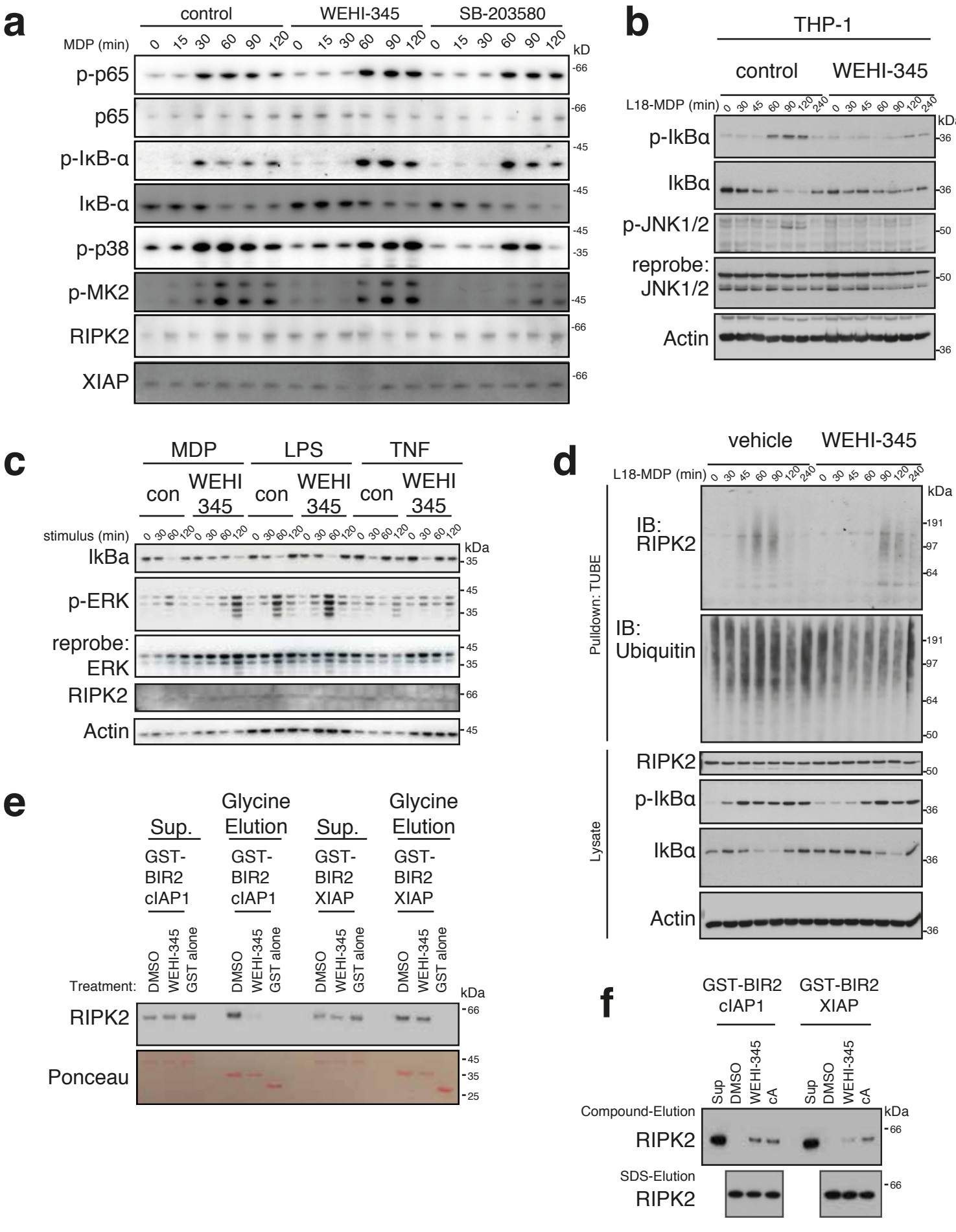

Nachbur et al, Figure 6

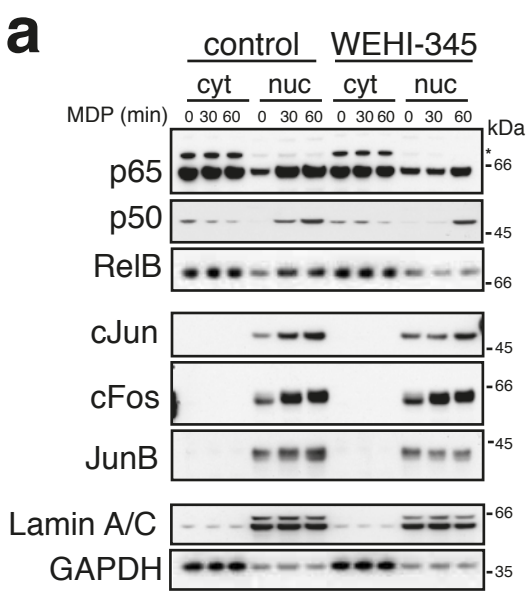

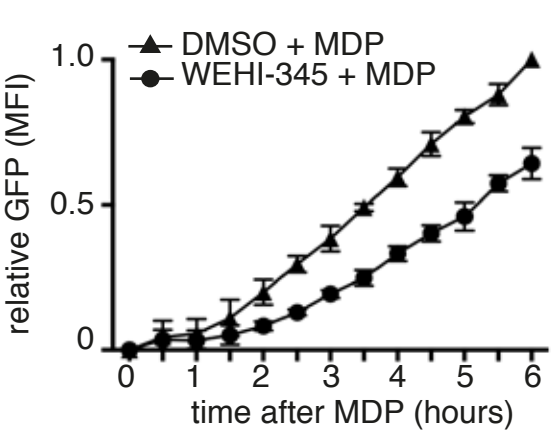

Nachbur et al, Figure 7

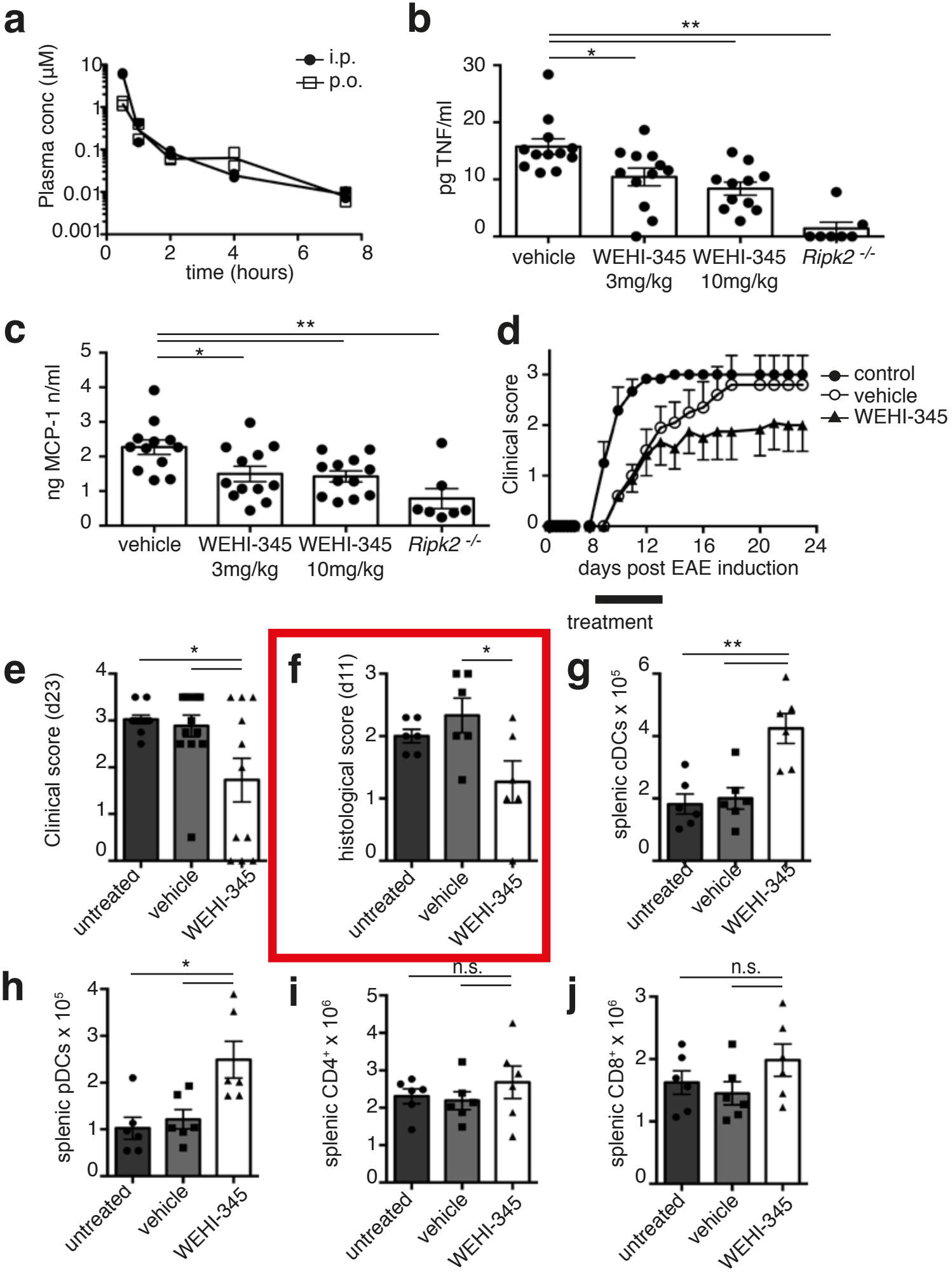

Nachbur et al, supplementary figure 1

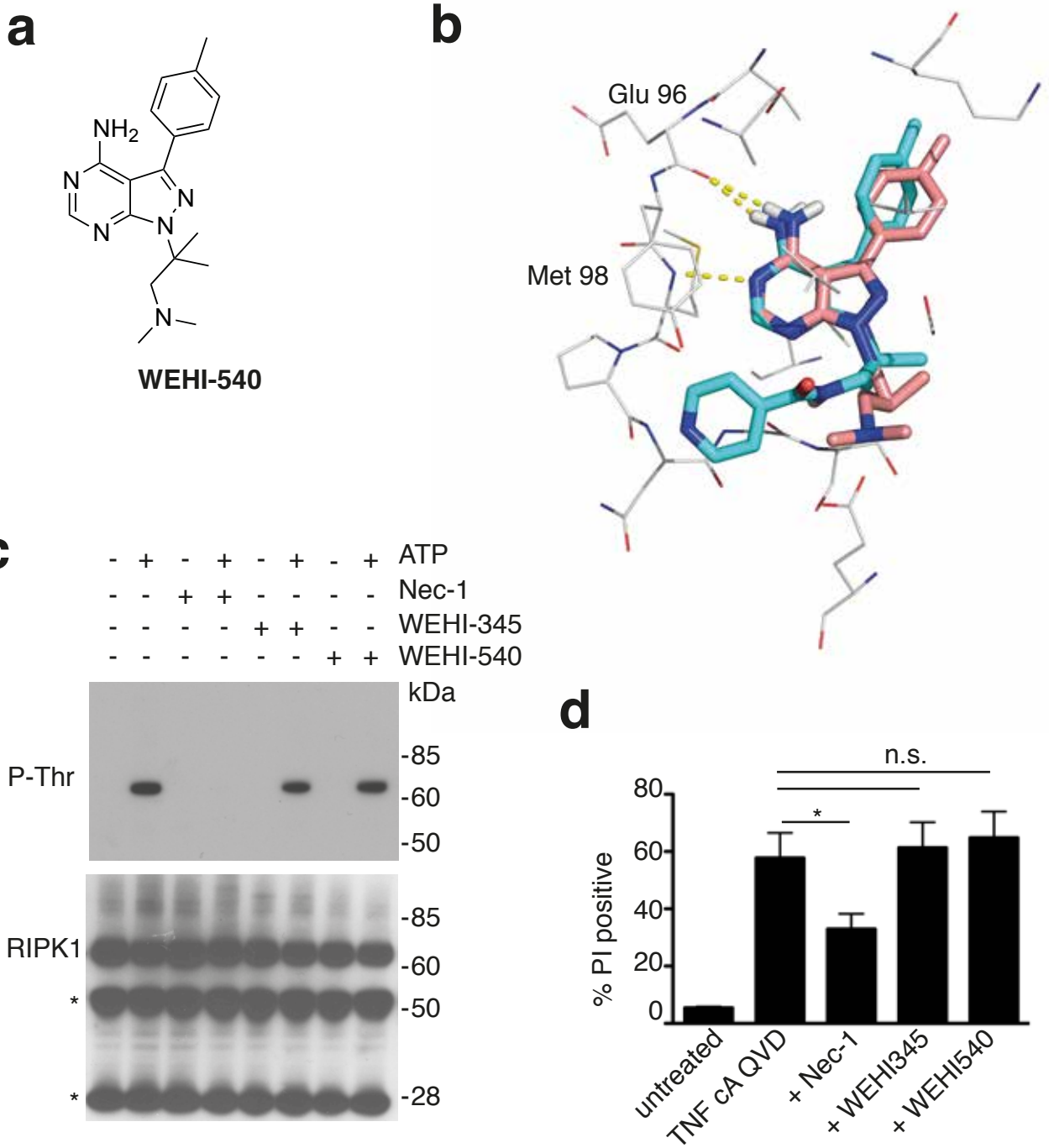

Nachbur et al, supplementary figure 2

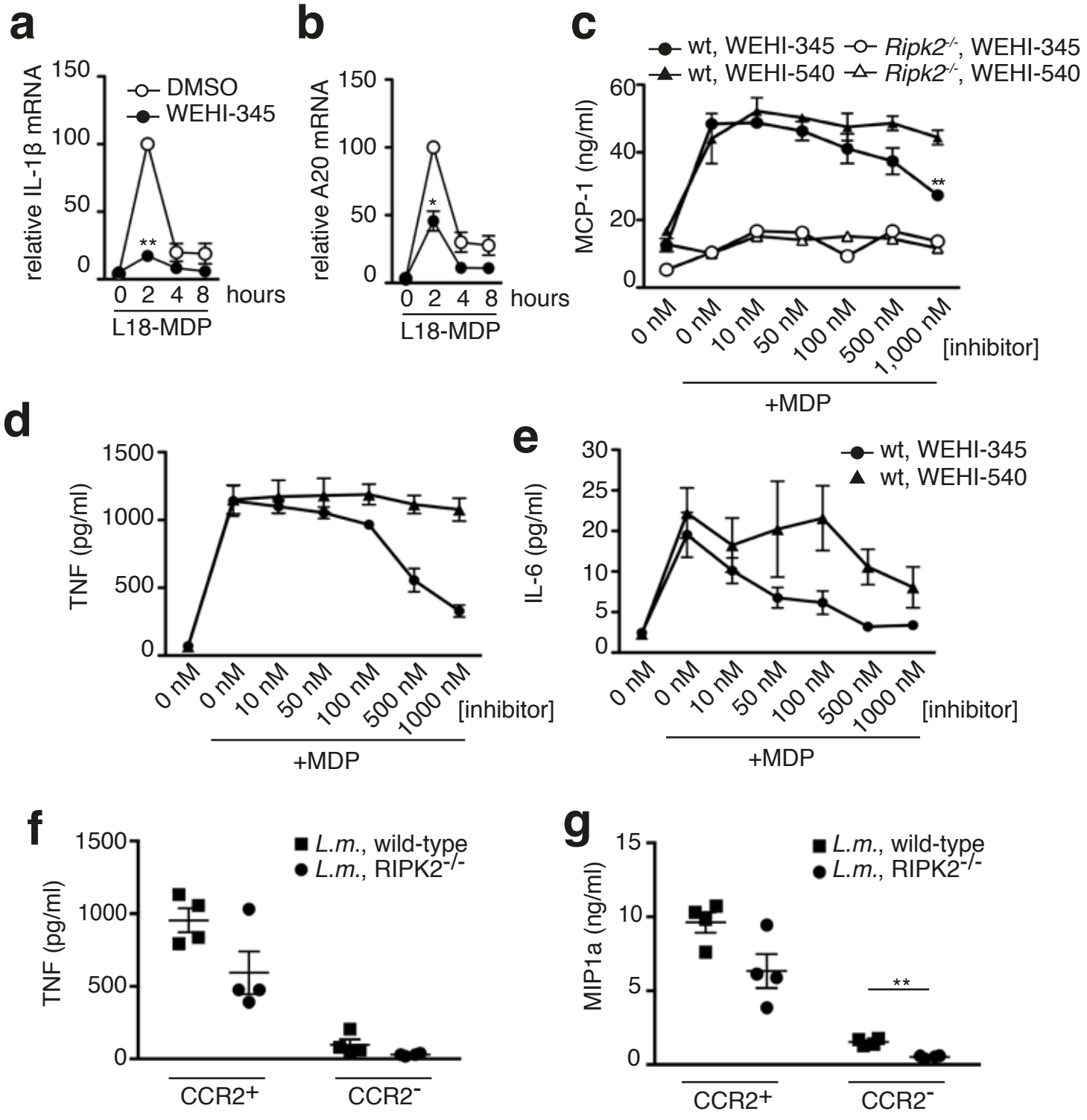

Nachbur et al, supplementary figure 3

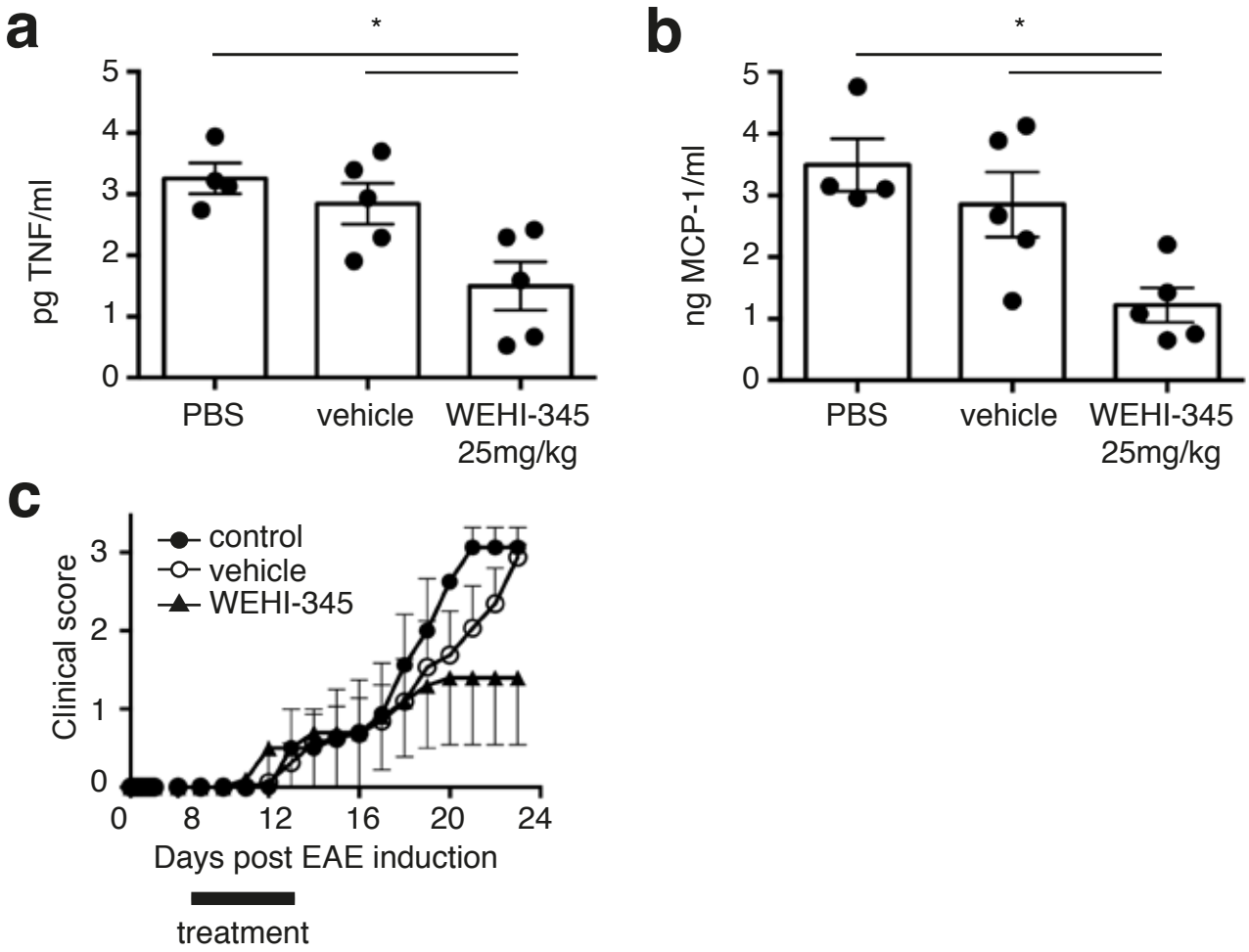

Nachbur et al, supplementary figure 4

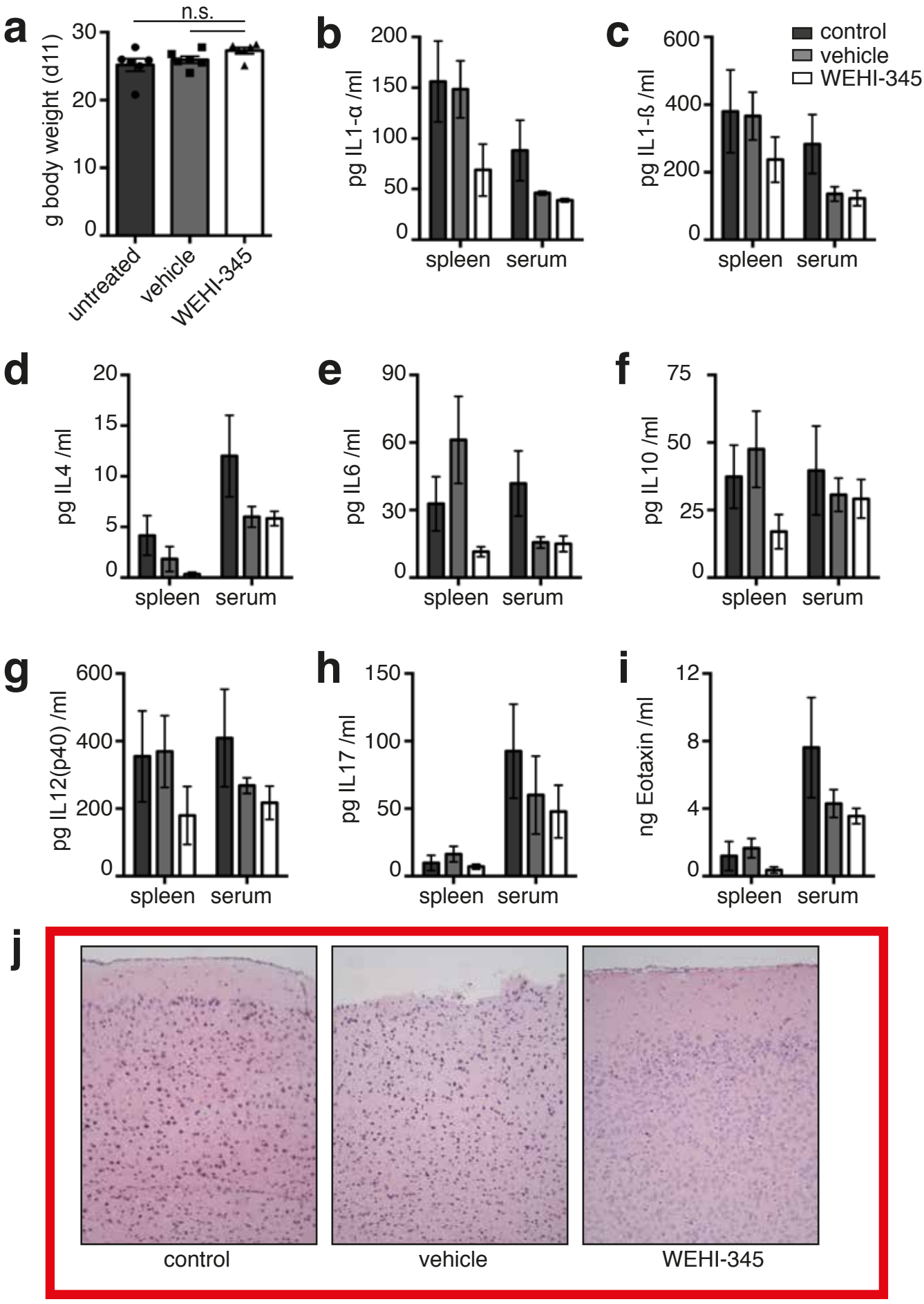

Nachbur et al, supplementary table1

KINOMEscan Gene Symbol	Entrez Gene Symbol	% activity	KINOMEscan Gene Symbol	Entrez Gene Symbol	% activity
ABL1(E255K)-phosphorylated	ABL1	31	KIT(V559D,T670I)	KIT	75
ABL1(T315I)-phosphorylated	ABL1	100	LKB1	STK11	100
ABL1-phosphorylated	ABL1	34	MAP3K4	MAP3K4	93
ACVR1B	ACVR1B	100	MAPKAPK2	MAPKAPK2	100
ADCK3	CABC1	96	MARK3	MARK3	85
AKT1	AKT1	100	MEK1	MAP2K1	66
AKT2	AKT2	100	MEK2	MAP2K2	75
ALK	ALK	65	MET	MET	100
AURKA	AURKA	100	MKNK1	MKNK1	31
AURKB	AURKB	63	MKNK2	MKNK2	100
AXL	AXL	66	MLK1	MAP3K9	97
BMPR2	BMPR2	75	p38-alpha	MAPK14	100
BRAF	BRAF	87	p38-beta	MAPK11	100
BRAF(V600E)	BRAF	42	PAK1	PAK1	88
BTK	BTK	86	PAK2	PAK2	82
CDK11	CDK19	94	PAK4	PAK4	100
CDK2	CDK2	100	PCTK1	CDK16	100
CDK3	CDK3	100	PDGFRA	PDGFRA	69
CDK7	CDK7	72	**PDGFRB**	**PDGFRB**	**2.8**
CDK9	CDK9	96	PDPK1	PDPK1	98
CHEK1	CHEK1	100	PIK3C2B	PIK3C2B	100
CSF1R	CSF1R	69	PIK3CA	PIK3CA	100
CSNK1D	CSNK1D	60	PIK3CG	PIK3CG	100
CSNK1G2	CSNK1G2	95	PIM1	PIM1	100
DCAMKL1	DCLK1	100	PIM2	PIM2	47
DYRK1B	DYRK1B	83	PIM3	PIM3	100
EGFR	EGFR	74	PKAC-alpha	PRKACA	100
EGFR(L858R)	EGFR	83	PLK1	PLK1	100
EPHA2	EPHA2	100	PLK3	PLK3	100
ERBB2	ERBB2	89	PLK4	PLK4	92
ERBB4	ERBB4	91	PRKCE	PRKCE	83
ERK1	MAPK3	90	RAF1	RAF1	83
FAK	PTK2	97	**RET**	**RET**	**0.4**
FGFR2	FGFR2	94	RIOK2	RIOK2	81
FGFR3	FGFR3	100	ROCK2	ROCK2	100
FLT3	FLT3	94	RSK2(Kin.Dom.1-N-terminal)	RPS6KA3	47
GSK3B	GSK3B	70	SNARK	NUAK2	100
IGF1R	IGF1R	91	SRC	SRC	6.1
IKK-alpha	CHUK	82	SRPK3	SRPK3	100
IKK-beta	IKBKB	44	TGFBR1	TGFBR1	50
INSR	INSR	100	TIE2	TEK	100
JAK2(JH1domain-catalytic)	JAK2	42	TRKA	NTRK1	100
JAK3(JH1domain-catalytic)	JAK3	100	TSSK1B	TSSK1B	100
JNK1	MAPK8	35	TYK2(JH1domain-catalytic)	TYK2	82
JNK2	MAPK9	100	ULK2	ULK2	83
JNK3	MAPK10	100	VEGFR2	KDR	99
KIT	**KIT**	**4.4**	YANK3	STK32C	100
KIT(D816V)	KIT	11	ZAP70	ZAP70	98

Nachbur et al, supplementary table 2

day	untreated (n=6)						vehicle (n=5)					WEHI-345 (n=6)					
0	0	0	0	0	0	0	0	0	0	0	0	0	0	0	0	0	0
1	0	0	0	0	0	0	0	0	0	0	0	0	0	0	0	0	0
2	0	0	0	0	0	0	0	0	0	0	0	0	0	0	0	0	0
3	0	0	0	0	0	0	0	0	0	0	0	0	0	0	0	0	0
4	0	0	0	0	0	0	0	0	0	0	0	0	0	0	0	0	0
5	0	0	0	0	0	0	0	0	0	0	0	0	0	0	0	0	0
6	0	0	0	0	0	0	0	0	0	0	0	0	0	0	0	0	0
7	0	0	0	0	0	0	0	0	0	0	0	0	0	0	0	0	0
8	0	0	0	0	0	0	0	0	0	0	0	0	0	0	0	0	0
9	0.5	0	1	2.5	1	2.5	0	0	0	0	0	0	0	0	0	0	0
10	2.75	0	2.5	3	2.75	2.75	0.5	1	0.5	0.5	0.5	1	0.5	0.5	0.5	0.5	0.5
11	3	1.5	2.75	3	2.75	3	1.5	1	0.5	0.5	1.5	2	0.5	1	0.5	0.5	1
12	3	2.5	3	3	3	3	2.5	2	0.5	0.5	2	2	0.5	2.5	0.5	0.5	2.5
13	3	2.5	3	3	3	3	2.75	2.5	0.5	1.5	2.5	2.5	0.5	2.75	0.5	1	2.75
14	3	3	3	3	3	3	2.75	2.5	0.5	2	2.5	2	0.5	2.75	0.5	1	2.5
15	3	3	3	3	3	3	2.75	3	0.5	2.5	2.5	2.5	0.5	2.75	0.5	2.5	2.5
16	3	3	3	3	3	3	2.5	3	0.5	3.5	2.25	2.5	0.5	2.75	0.5	2.75	1.5
17	3	3	3	3	3	3	3.5	3	0.5	3.5	2.5	3.5	0.5	2.75	0.5	3	1
18	3	3	3	3	3	3	3.5	3	0.5	3.5	3.5	3.5	0.5	2.75	0.5	3	1
20	3	3	3	3	3	3	3.5	3	0.5	3.5	3.5	3.5	0.5	2.5	0.5	3	1.5
21	3	3	3	3	3	3	3.5	3	0.5	3.5	3.5	3.5	0.5	2.75	0.5	3	2
22	3	3	3	3	3	3	3.5	3	0.5	3.5	3.5	3.5	0.5	2.5	0.5	3	2
23	3	3	3	3	3	3	3.5	3	0.5	3.5	3.5	3.5	0.5	2.5	0.5	3	2

Nachbur et al, supplementary table 3

day	untreated (n=4)				vehicle (n=8)								WEHI-345 (n=5)				
0	0	0	0	0	0	0	0	0	0	0	0	0	0	0	0	0	0
1	0	0	0	0	0	0	0	0	0	0	0	0	0	0	0	0	0
2	0	0	0	0	0	0	0	0	0	0	0	0	0	0	0	0	0
3	0	0	0	0	0	0	0	0	0	0	0	0	0	0	0	0	0
4	0	0	0	0	0	0	0	0	0	0	0	0	0	0	0	0	0
5	0	0	0	0	0	0	0	0	0	0	0	0	0	0	0	0	0
6	0	0	0	0	0	0	0	0	0	0	0	0	0	0	0	0	0
7	0	0	0	0	0	0	0	0	0	0	0	0	0	0	0	0	0
8	0	0	0	0	0	0	0	0	0	0	0	0	0	0	0	0	0
9	0	0	0	0	0	0	0	0	0	0	0	0	0	0	0	0	0
10	0	0	0	0	0	0	0	0	0	0	0	0	0	0	0	0	0
11	0	0	0	0	0	0	0	0	0	0	0	0	0.5	0	0	0	0
12	0	0	0	0	0	0	0	0	0	0.5	0	0	2.5	0	0	0	0
13	0	0	2	0	0	0	0	0	0	2	0.5	0	2.5	0	0	0	0
14	0	0	2	0	0	0	0	0	0	2.5	2	0	3.5	0	0	0	0
15	0	0	2.5	0	0	0	0	0	0	2.5	2.5	0	3.5	0	0	0	0
16	0	0	2.75	0	0	0	0	0	0	2.75	2.75	0	3.5	0	0	0	0
17	0	0	2.75	1	0	0	0	0	1	2.75	3	0	3.5	1	0	0	0
18	1	0	2.75	2.5	0	0	0	0	2.5	2.75	3.5	0	3.5	2	0	0	0
19	2.75	0	2.75	2.5	0	0	0	0	3.5	2.75	3.5	2.5	3.5	3	0	0	0
20	2.75	2.5	2.75	2.5	0	0	1	0	3.5	2.75	3.5	2.75	3.5	3.5	0	0	0
21	3.5	3.5	2.75	2.5	1	0	2	0	3.5	2.75	3.5	3.5	3.5	3.5	0	0	0
22	3.5	3.5	2.75	2.5	2	1	2.5	0	3.5	2.75	3.5	3.5	3.5	3.5	0	0	0
23	3.5	3.5	2.75	2.5	2.75	2.5	2.5	2.5	3.5	2.75	3.5	3.5	3.5	3.5	0	0	0